Global defects in collagen secretion in a *Mia3/TANGO1* knockout mouse

Deanna G. Wilson,[1] Khanhky Phamluong,[1] Li Li,[2] Mei Sun,[3] Tim C. Cao,[4] Peter S. Liu,[5] Zora Modrusan,[1] Wendy N. Sandoval,[5] Linda Rangell,[3] Richard A. D. Carano,[4] Andrew S. Peterson,[1] and Mark J. Solloway[1]

[1]Department of Molecular Biology, [2]Department of Bioinformatics and Computational Biology, [3]Department of Pathology, [4]Department of Research Oncology, and [5]Department of Protein Chemistry, Genentech, South San Francisco, CA 94080

Melanoma inhibitory activity member 3 (MIA3/TANGO1) is an evolutionarily conserved endoplasmic reticulum resident transmembrane protein. Recent in vitro studies have shown that it is required for the loading of collagen VII, but not collagen I, into COPII-coated transport vesicles. In this paper, we show that mice lacking Mia3 are defective for the secretion of numerous collagens, including collagens I, II, III, IV, VII, and IX, from chondrocytes, fibroblasts, endothelial cells, and mural cells. Collagen deposition by these cell types is abnormal, and extracellular matrix composition is compromised. These changes are associated with intracellular accumulation of collagen and the induction of a strong unfolded protein response, primarily within the developing skeleton. Chondrocyte maturation and bone mineralization are severely compromised in *Mia3*-null embryos, leading to dwarfism and neonatal lethality. Thus, Mia3's role in protein secretion is much broader than previously realized, and it may, in fact, be required for the efficient secretion of all collagen molecules in higher organisms.

Introduction

Protein synthesis in secretory cells is exquisitely regulated to meet the changing demands for secreted proteins that participate in physiological and developmental processes. One example of developmentally regulated cells with extraordinary secretory capacity are the chondrocytes of the developing skeleton, which differentiate from a simple mesenchymal condensation to a highly ECM-enriched group of cells within 24 h. Effectors of protein folding and transport are necessarily up-regulated to cope with the increased protein load and support the transition to a highly secretory phenotype. Concomitantly, the synthesis and secretion of collagens and other ECM proteins that comprise the cartilage matrix are also dynamically regulated as the skeleton grows and develops.

The collagens are a large family of structural proteins that form diverse supramolecular assemblies within the ECM throughout the body and skeleton. These proteins are defined by a repeating Gly-X-Y motif in the pro–α chains, which associate in the ER into a triple helix (Lamandé and Bateman, 1999). The general process of synthesis, assembly, and formation of the helical domain is similar for all collagens. Collagen precursors are co-translated into the ER, where secondary modifications occur that are essential for oligomerization and stabilization by the ER-resident collagen chaperone Hsp47. Trimers are exported from the ER and trafficked through the Golgi network, where they are further modified by N-linked oligosaccharide addition before secretion into the extracellular space and organization into higher order structures.

The mean fibrillar collagen, when formed into a trimer, adopts a rigid, rodlike structure of >300 nm in length. This is too large to fit into typical 60–80-nm ER–Golgi transport vesicles enshrouded by the COPII coat protein, sparking a controversy as to whether a new vesicular transport model needs to be invoked (Fromme and Schekman, 2005). Procollagens are segregated at ER exit sites into large transport complexes that are distinct from typical smaller ER vesicles labeled by ERGIC-53 and VSVG (vesicular stomatitis virus G) protein (Stephens and Pepperkok, 2002). More specifically, in chondrocytes, the

D.G. Wilson and K. Phamluong contributed equally to this paper.

Correspondence to A.S. Peterson: peterson.andrew@gene.com; or M.J. Solloway: solloway.mark@gene.com

Abbreviations used in this paper: dpc, day postcoitum; ERAD, ER-associated degradation; MEF, mouse embryonic fibroblast; MI, myocardial infarct; micro-CT, microcomputed tomography; PNGase F, peptide-*N*-glycosidase F; TEM, transmission EM; UPR, unfolded protein response; wt, wild type.

The Rockefeller University Press $30.00
J. Cell Biol. Vol. 193 No. 5 935–951
www.jcb.org/cgi/doi/10.1083/jcb.201007162

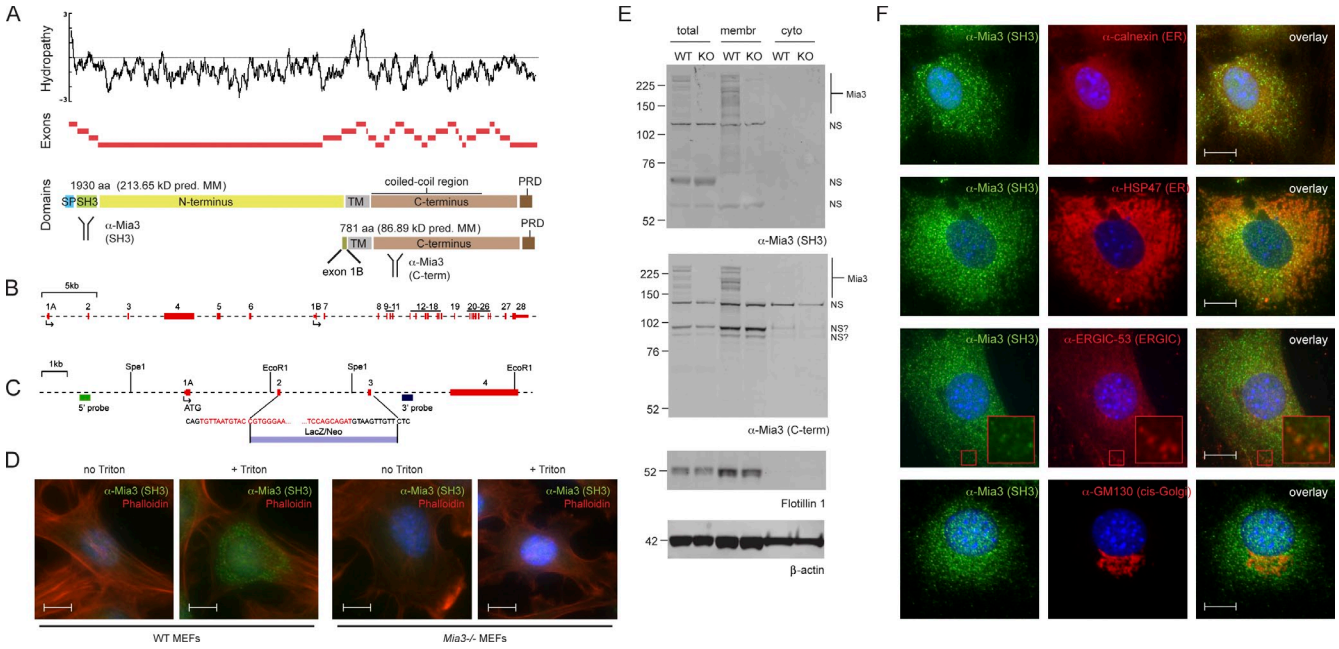

Figure 1. **Mia3 is an ER-associated protein.** (A) Hydropathy chart, exon alignment, and proposed domain structure of Mia3 with two antibody (α-Mia3) epitopes indicated. SP, signal peptide; SH3, putative SH3-like fold; TM, transmembrane domain; PRD, proline-rich domain; pred. MM, predicted molecular mass. (B and C) Mia3 intron/exon map and description of the targeted allele. Nucleotides highlighted in red correspond to exon2 and exon3 sequences. LacZ/neo, LacZ/neomycin. (D) α-Mia3 SH3 polyclonal antibodies show punctate intracellular staining that is absent in *Mia3*-null MEFs or nonpermeabilized cells. (E) Western blot analysis of total protein, membrane (membr), and cytosolic (cyto) fractions from wt and *Mia3*$^{-/-}$ 14.5-dpc embryos reveals two major bands near 250 kD with several smaller isoforms or degradation products in the membrane fraction. NS, nonspecific antibody cross-reactivity; C-term, C terminus; KO, knockout. Molecular masses are given in kilodaltons. (F) Immunofluorescent colocalization analyses of α-Mia3 SH3 with antibodies against calnexin, Hsp47 (SerpinH1), ERGIC-53 (Lman1), and GM130 in primary chondrocytes reveals an Mia3 protein within punctate structures on the ER membrane. Insets detail regions boxed in red. Bars, 10 µm.

distribution of aggrecan, another large secreted ECM glycoprotein, has a localization distinct from that of Col2a1 (collagen II) in the ER (Vertel et al., 1989), which strongly suggests that collagens are actively packaged by specific cargo receptors and/or chaperones within a unique compartment.

A genome-wide RNAi screen using insect cells to identify transport components and other factors required for Golgi organization (TANGO [transport and Golgi organization] genes) led to the identification of the *Drosophila melanogaster* homologue of the vertebrate gene *MIA3*, also known as TANGO1 (Bard et al., 2006). MIA3 is a unique 1,907 amino acid protein, which has recently been proposed to act as an ER-resident chaperone for Col7a1 (collagen VII; Saito et al., 2009b) based on elegant biochemical and cell biological analyses. Saito et al. (2009b) found that Mia3 spans the ER membrane and binds Col7a1 via an SH3 (Src homology 3)-like fold residing within the ER lumen, whereas on the cytoplasmic face, a C-terminal proline-rich domain binds the Sec23 and Sec24 proteins of the COPII coat complex. This dual interaction is hypothesized to facilitate the generation and packaging of ER megavesicles of sufficient size to support the transport of the bulky Col7a1 trimer. Intriguingly, they also found that knockdown of MIA3 failed to affect the secretion of Col1 (collagen I), suggesting that MIA3 was required for efficient packaging of only a subset of collagens.

Providing another clue toward the function of Mia3, unbiased genetic analyses of heart disease in human patients have linked a single-nucleotide polymorphism in *MIA3* with coronary artery disease and early onset myocardial infarct (MI; Samani et al., 2007; Kathiresan et al., 2009). Down-regulation of *MIA3* has been observed in malignant melanoma (Arndt and Bosserhoff, 2006) as well as colon and hepatocellular carcinomas (Arndt and Bosserhoff, 2007), but it remains unclear whether these changes are epiphenomena, are causative, or are correlates of cancerous progression without an active role. Despite this intriguing set of observations, it has not been possible to tie these disparate results together into a clear picture of the function of Mia3.

To clarify its function, we generated a null allele of *Mia3* in the mouse. *Mia3* knockouts display a chondrodysplasia that causes dwarfing of the fetus, peripheral edema, and perinatal lethality. Further analysis reveals a substantial shift in collagen metabolism, likely resulting from delayed transit through the secretory pathway. This phenotype combines aspects of several different diseases caused by defects in collagen production. Our analysis highlights the sensitivity of the chondrogenic/skeletogenic processes to defects in protein secretion and further suggests that regulators of ER and Golgi function may be causative in cases of recessive chondrodysplasias that remain as yet unmapped. The generalized role of Mia3 in escorting all collagens examined to date, including collagens I, II, III, IV, VII, and IX, but not other ECM components, such as fibronectin or aggrecan, indicates that this protein plays a unique role within the cell to facilitate the nucleation of large ER transport vesicles dedicated to the export of collagens and perhaps collagen-associated molecules of the ECM.

Table I. **Onset and penetrance of the *Mia3*-null phenotype**

Stage	Wt	Heterozygote	Homozygote	Null allele
dpc				%
10.5	12	22	11	24.4
12.5	49	95	43	23
13.5[a]	81	162	87	26.4
14.5	92	212	86	22.1
15.5[b]	63	110	44	20.3
16.5	10	13	6	20.7
18.5	10	19	14	32.6

Embryo recovery and genotype distribution from $Mia3^{+/-}$ heterozygous intercrosses collected from 10.5–18.5 dpc.
[a]Differences first apparent by marker analysis.
[b]Overt phenotype first apparent (100% penetrance).

Results

To elucidate the role of MIA3 in vivo, we characterized the phenotype of a *Mia3* knockout mouse. Mia3 contains a putative signal peptide, an N-terminal SH3 domain followed by two coiled-coil domains, a transmembrane domain, and a C-terminal proline-rich domain (Fig. 1 A). A gene-targeting cassette encoding a LacZ/neomycin fusion protein was inserted in frame 11 bases into the beginning of the second exon, replacing the contents of this exon and all of exon3 (Fig. 1, B and C). This vector deletes the SH3 domain that has been shown to mediate interactions with Col7a1 (Saito et al., 2009b). Correct targeting events were confirmed by Southern blot analysis using both 5′ and 3′ genomic probes as well as PCR (Fig. S1 A).

Cross-species alignments suggest the existence of an alternate promoter and coding exon within the sixth intron, which we refer to as exon1B (Fig. 1, A and B). cDNAs initiating in this exon are present in both mouse and human genomes (University of California Santa Cruz Genome Browser), and numerous ESTs joining exons 1B and 7 confirm that this is a valid transcript. We further verified this by cloning exon 1B–7 fusion transcripts by RT-PCR from both wild-type (wt) and knockout embryos (Fig. S1 B). Translation of this hypothetical protein initiates in frame immediately before the transmembrane domain of full-length Mia3 but lacks a well-defined signal peptide (SignalP 3.0; ExPASy proteomics server). Given that the COPII-binding proline-rich domain is present in this isoform, it is possible that it has a cytoplasmic role that is distinct from the proposed ER cargo-binding role of full-length Mia3. To address this issue, affinity-purified rabbit polyclonal antibodies were raised against the purified SH3 domain as well as a linear peptide within the C-terminal tail. Immunohistochemical staining of 14.5–d postcoitum (dpc) embryonic limbs with the anti-SH3 antibody demonstrates expression in many cell types, which is absent from knockout embryos (Fig. S2 A). Immunofluorescence labeling of wt and *Mia3*-null mouse embryonic fibroblasts (MEFs) with the anti-SH3 antibody reveals punctate staining peripheral to the nucleus only upon permeabilization and only in wt cells (Fig. 1 D). The C-terminal antibody gives a similar pattern of staining (Fig. S2 B), and the signal from the two antibodies is perfectly colocalized (Fig. S2 C).

To further delineate the subcellular localization of Mia3, cytosolic and membrane fractions of wt and mutant embryos were compared using SDS-PAGE and Western blotting (Fig. 1 E). Mia3 contains eight putative N-linked glycosylation sites, and multiple high molecular mass bands (>150 kD) were observed with both antibodies, which is consistent with the presence of multiple isoforms and/or posttranslational modifications of Mia3. These bands are missing from the mutant embryos, verifying that we have eliminated expression of the large SH3 domain–containing isoform of Mia3. Two bands migrating at ∼80–90 kD are seen with the C-terminal antibody in both wt and mutant cells. These are close to the expected size of the truncated Mia3 isoform (molecular mass of 86.9 kD) predicted by an alternate promoter upstream of exon1B (Fig. 1 C). Mass spectrometry of immunoprecipitates from embryonic tissue using the C-terminal antibody confirms the absence of the larger SH3 domain–containing isoform in mutant lysates and the presence of the smaller SH3 domainless isoform in both mutant and wt animals (Fig. S1 E).

Immunofluorescent detection of Mia3 in primary chondrocytes and MEFs using the polyclonal anti-SH3 antibody reveals that Mia3 is present in regions demarcated by the ER-resident proteins calnexin and HSP47 (Fig. 1 F). ERGIC-53 domains are adjacent but mostly nonoverlapping with Mia3, and Mia3 is very weakly detected in the region delineated by the cis-Golgi marker GM130. These results are consistent with the observations of Saito et al. (2009b), and we conclude that Mia3 resides primarily on the ER membrane and does not transit through the Golgi apparatus.

Mice carrying a single targeted allele ($Mia3^{+/-}$) are fertile and show no gross evidence of haploinsufficiency. Homozygous mice, although recovered in the expected Mendelian frequencies, exhibit short-limbed dwarfism and die at birth (100% penetrant; Table I). Neonates fail to breathe and are often edemic with subdermal microhemorrhages. Skin and other tissues were noted to be particularly fragile during dissection. $Mia3^{-/-}$ embryos first appear morphologically distinct at 15.5–16.5 dpc (Fig. 2, A and B) with shortening of the snout and limbs, a subtle reduction in stature, and apparent tightening of the normally wrinkled dermis. These hallmarks of the mutant phenotype are preserved at 18.5 dpc, and the body axis is further shortened by ∼50% respective to controls (Fig. 2, C and D).

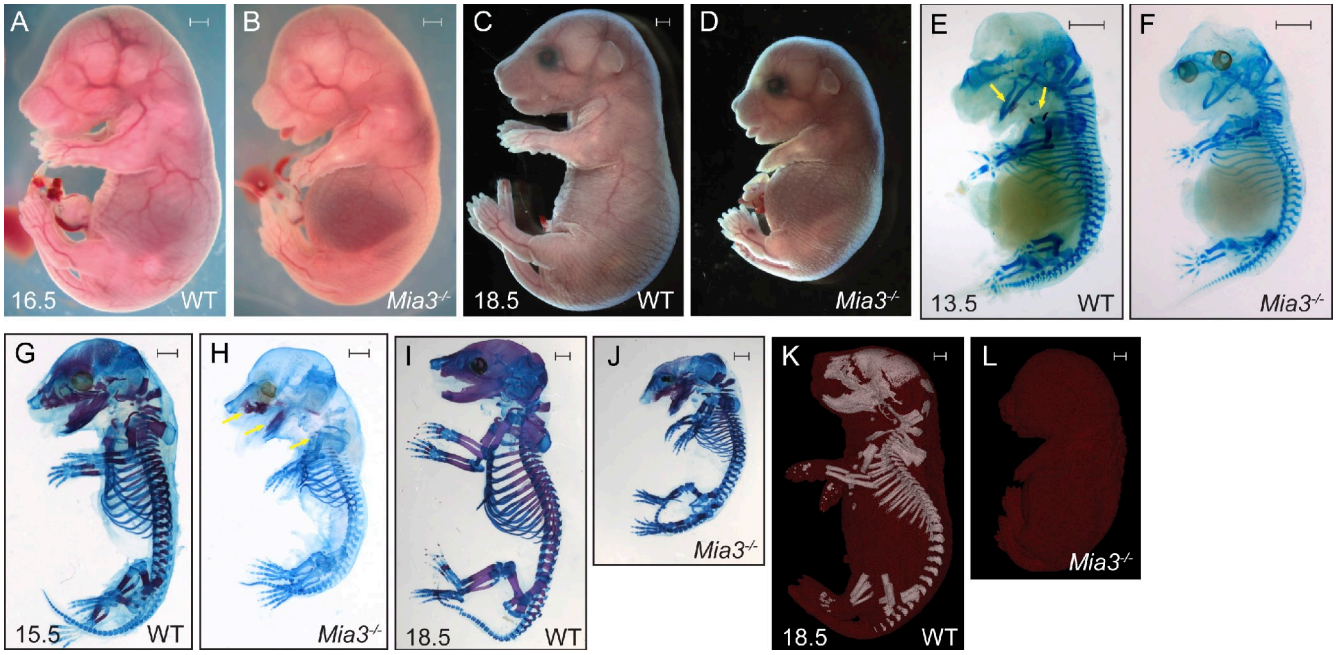

Figure 2. ***Mia3*$^{-/-}$ embryos are dwarfed, edemic, and fail to form a mineralized skeleton.** (A and B) *Mia3* mutant embryos display a shortening of the snout and limbs at 16.5 dpc. (C and D) *Mia3* mutant embryos are significantly dwarfed at 18.5 dpc. (E and F) Alizarin red–positive skeletal mineralization initiates within the intramembranous bone of the jaw and endochondral bones of the clavicles of 13.5-dpc wt embryos (arrows) but is absent from the Alcian blue–positive cartilage anlagen of *Mia3* mutants. (G and H) Mineralization is advanced in nearly all axial and appendicular elements in 15.5-dpc control embryos but is profoundly delayed in the *Mia3*-null skeleton. (I–L) Calcified matrix is apparent in the bones of 18.5-dpc knockout animals (I and J), but micro-CT (n = 3) maximum intensity projections highlight complete absence of the mature ossified skeleton (K and L). Bars, 1 mm.

Alizarin red/Alcian blue–stained skeletal preparations show that relative position and numbers of skeletal elements are normal, but a delay in the onset of mineralization is apparent at 13.5 dpc (Fig. 2, E and F), and there is an almost complete lack of calcium deposits at 15.5 dpc (Fig. 2, G and H), a time when the majority of skeleton components have initiated primary mineralization.

Residual mineral deposition is apparent in the dwarfed mutants at 18.5 dpc (Fig. 2, I and J), but microcomputed tomography (micro-CT) fails to detect ossified tissue, which would indicate secondary mineralization in the mutants (n = 3; Fig. 2, K and L). Secondary mineralization is driven by osteoblasts, and indeed, *Mia3* mutants have a severe reduction in *osteopontin* (*Spp1*)-positive osteoblasts at 14.5 dpc (Fig. 3, A and B) and show no detectable staining for osteoblast-derived Col1a1 and Igfbp6 (insulin-like growth factor–binding protein) in the perichondrium at this stage (not depicted). The few osteoblasts observed in the mutant bones were found primarily in the periphery of the perichondrium adjacent to the hypertrophic region at the middle of the condensation (Fig. 3 B). In the controls, these cells are well entrenched in the perichondrium and have invaded the remodeling matrix of the hypertrophic zone by 14.5 dpc (Fig. 3 A). Expression of Mmp9 (matrix metallopeptidase 9), a secreted ECM-degrading enzyme, which primes the mineralized matrix for vascular invasion (Vu et al., 1998), is strongly down-regulated (Fig. 3, C and D), and MECA-32–positive vessels are not apparent in the mutant hypertrophic zone. Clearly, the dependence of osteoblasts on Mia3 is not absolute, and by 16.5 dpc more, osteoblasts are apparent within the center of each bone, although their numbers are still drastically reduced with respect to wt littermates (Fig. 3, F and H), and they are restricted to the marrow cavity immediately underlying the Mmp9-positive perichondrium (Fig. 3, E and G). Thus, the absence of secondary mineralization is caused by severe defects in vascular invasion and recruitment of osteoblasts in *Mia3* mutants. We hypothesized that this was caused by a general delay in chondrogenic maturation and focused our further analysis on this.

Histological analysis confirmed the chondrogenic delay and highlighted defects in chondrocytic ECM deposition. Cartilaginous templates of the bone first become morphologically distinct in the *Mia3* mutants at 13.5 dpc (Fig. 3, I and J). In controls, Masson's trichrome stain reveals collagen deposition typical of maturing chondrocytes that begin to secrete increasing amounts of collagen and other structural proteins in the ECM (Fig. 3 I; Kronenberg, 2003). However, very little stain is seen in the mutants (Fig. 3 J). This is not simply because of a delay in cellular differentiation, as the ECM stain surrounding the hypertrophic cells is still significantly reduced in the mutant embryos at 15.5 dpc (Fig. 3, K and L). Mineralized bone collar, which is stained darkly blue, is embedded in the perichondrium of controls at this stage but missing from the mutants. Hematoxylin and eosin–stained sections of *Mia3*$^{-/-}$ humeri show a complete absence of well-defined trabeculae seen at the diaphysis of controls (Fig. 3, M and N). Ki67 labeling of 14.5-dpc humeri indicates that chondrocytes populating the resting and proliferative zones maintain their proliferative capacity in the knockout mice (Fig. 4, A, B, and I). However, consistent with the arrest in chondrogenic progression, dying TUNEL-positive cells are completely absent from the center of the mutant bone (Fig. 4, E and F). By 16.5 dpc, the majority of cells residing

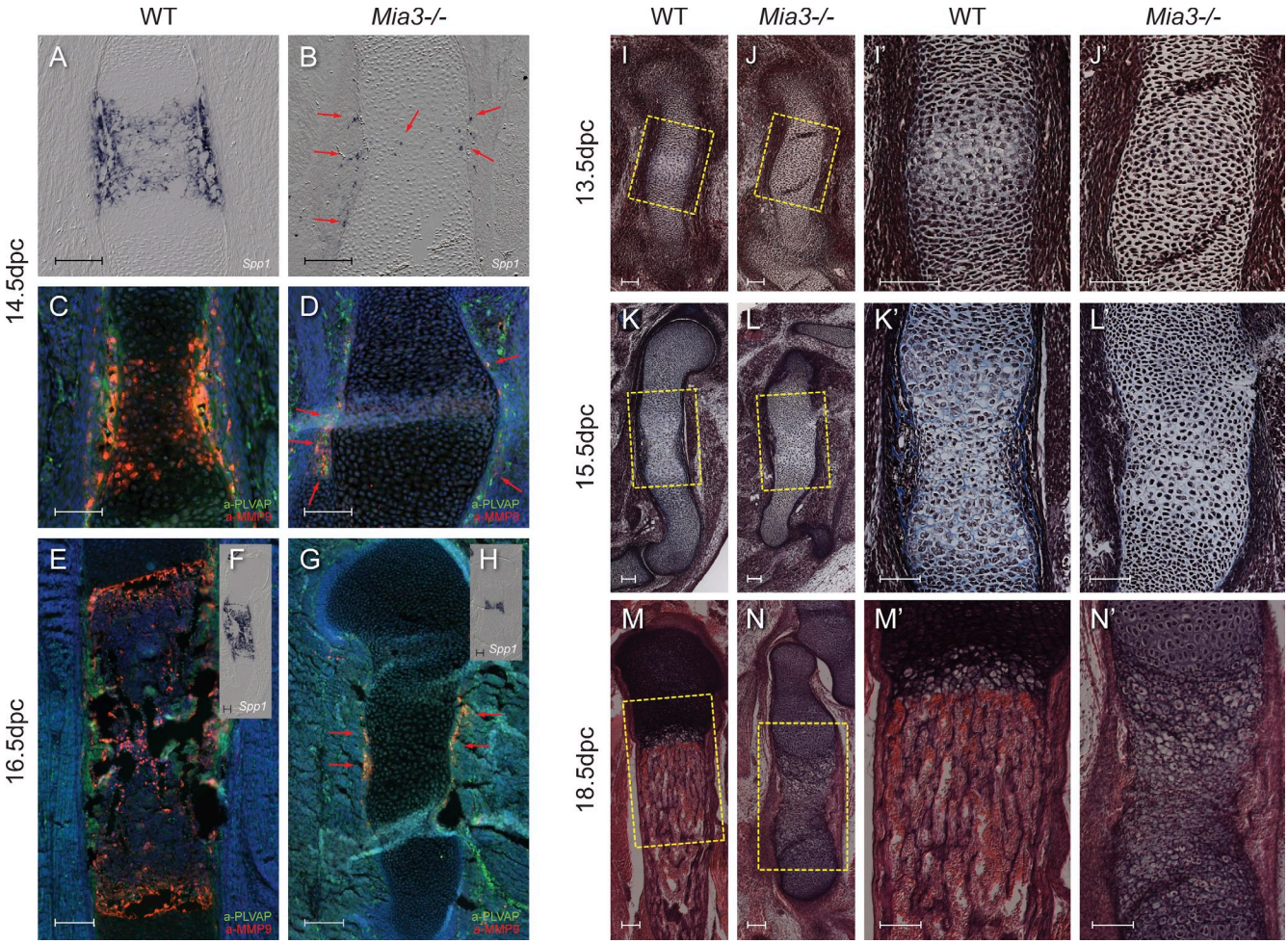

Figure 3. **Osteogenesis is compromised by the delay in chondrogenic progression and vascular recruitment in *Mia3*-null bone.** (A and B) In contrast to wt embryos, rare *Spp1*-positive osteoblasts (arrows) are present in the perichondrium of the *Mia3*$^{-/-}$ humerus at 14.5 dpc. (C and D) Mmp9 and PLVAP/MECA-32 are restricted to a few cells within the perichondrium of *Mia3*$^{-/-}$ bones at 14.5 dpc. (E and G) At 16.5 dpc, Mmp9-positive cells remain restricted to the presumptive bone collar perichondrium of *Mia3* mutant embryos. (F and H) A small number of *Spp1*-positive osteoblasts reside within the hypertrophic zone. (I–N′) Masson's trichrome stain (I–L) and hematoxylin/eosin stain (M and N) of wt and *Mia3*-null humeri at 13.5, 15.5, and 18.5 dpc highlight the onset and progression of the chondrodysplastic phenotype. Boxed regions (I–N) are enlarged to the right of each set of panels (I′–N′). Bars, 100 µm.

internal to the bone collar are Ki67 positive, whereas in the mutant, the terminally differentiated chondrocytes remain unlabeled (Fig. 4, C and D), and a small number of these are now TUNEL positive (Fig. 4, G and H). Dying cells are not apparent elsewhere in the mutant bone. Thus, the generalized dwarfing of the knockout skeleton is driven primarily by the delay and arrest of chondrogenic maturation, lack of vascular recruitment, and the failure to elaborate a primary ossification center in *Mia3* mutants.

We characterized the delay in chondrogenic progression by examining the expression of chondrocyte differentiation markers and major signaling pathways involved in chondrogenesis. At 14.5 dpc, mature hypertrophic chondrocytes expressing *Col10a1* (*collagen type X*) in the absence of *Col2a1* (*collagen type II*) and *Col9a1* (*collagen type IX*) are evident at the center of the control bone anlagen, whereas adjacent prehypertrophic cells express all three collagens (Fig. 4, J–O). *Col10a1* expression initiates in the center of the *Mia3* mutant bone as well, but these cells also maintain expression of *Col2a1* and *Col9a1* and are, thus, in the prehypertrophic stage. *Ihh* (*Indian hedgehog*) is also expressed by these cells and required for proper chondrocyte maturation (St-Jacques et al., 1999; Long et al., 2001). Despite the delay in chondrogenic maturation, *Ihh* and its downstream target/effector gene *Ptc* (*patched*) are correctly restricted to the proliferating chondrocytes and perichondrium (Fig. 4, P–S). Expression of the parathyroid hormone–related protein receptor *Pth1r*, normally restricted to prehypertrophic cells, further confirms the overall delay in chondrocyte maturation (Fig. 4, T and U). The delay was substantiated by microarray analysis comparing 14.5-dpc wt and mutant limb buds (Fig. 4, V and W). Thus, we conclude that major signaling axes involved in chondrocytic maturation are preserved in *Mia3*-null bones despite profound defects in chondrocytic differentiation.

The preservation of major signaling pathways in the mutant led us to assess the role of Mia3 in chondrocyte differentiation more directly. We generated primary MEFs from mutant and wt embryos, cultured them under chondrogenic conditions for 2 wk, and assessed the expression of *Col2a1* and *Col10a1* by TaqMan PCR (Fig. S3, A and B). *Col2a1* is ordinarily expressed

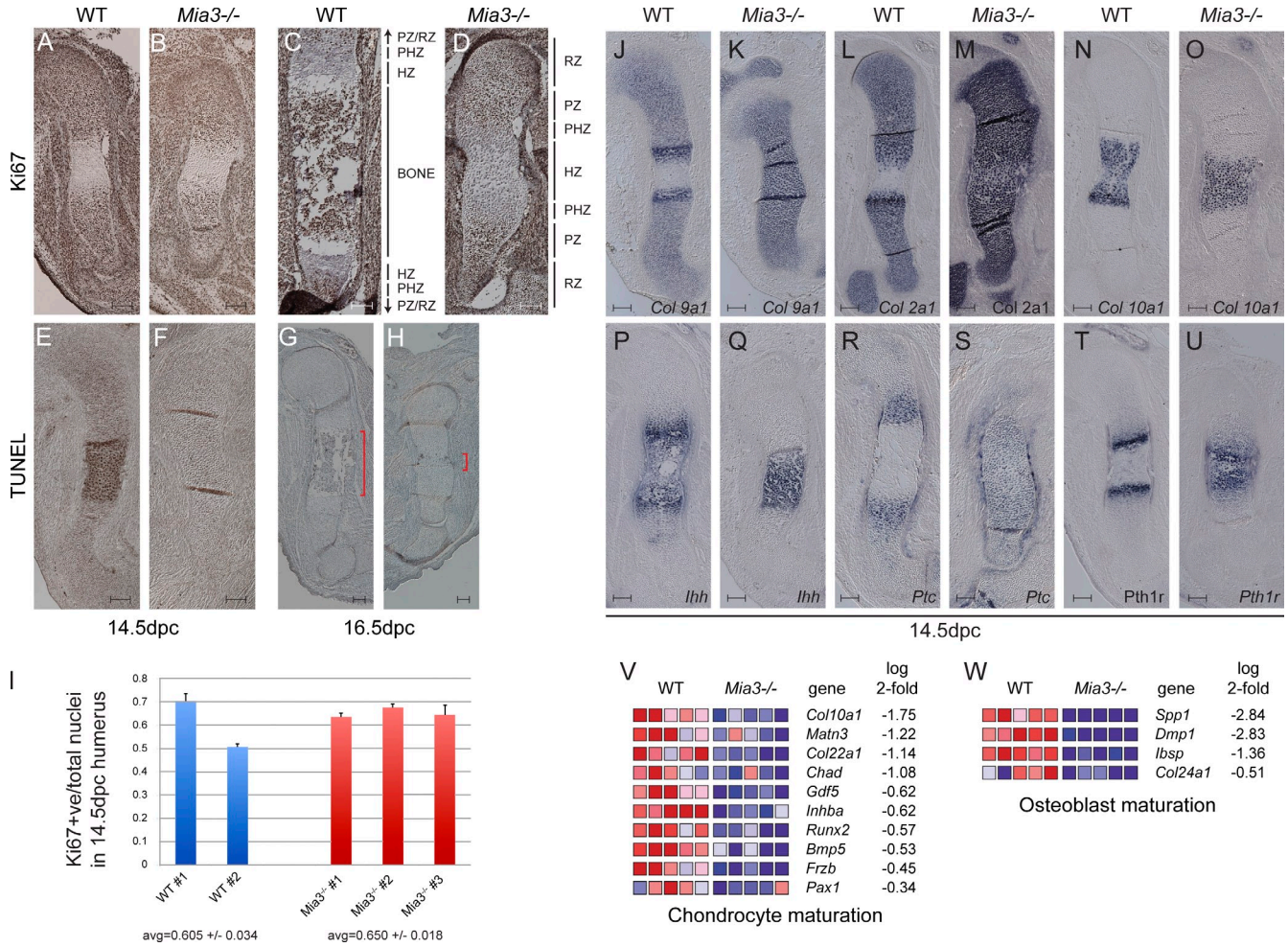

Figure 4. **Early chondrocyte proliferation, differentiation, and critical patterning pathways are preserved in 14.5-dpc humeri despite abnormal chondrocyte morphology in *Mia3*$^{-/-}$ embryos.** (A–D) Ki67 labeling of 14.5-dpc (A and B) and 16.5-dpc (C and D) humeri demonstrate normal proliferation of mutant chondrocytes. RZ, PZ, PHZ, and HZ denote resting, proliferative, prehypertrophic, and hypertrophic zones, respectively. (E and F) The majority of terminally differentiated hypertrophic chondrocytes are TUNEL positive in wt 14.5-dpc humeri (E), whereas *Mia3*-null hypertrophic chondrocytes fail to die (F). (G and H) Scattered dying cells are restricted to the hypertrophic zone in 16.5-dpc wt and *Mia3*-null humeri (red brackets). (I) Ki67-positive (+ve) cells within the proliferative zone. Mean values are presented, and SEM is shown from two independent wt samples and three Mia3$^{-/-}$ humeri with 4–10 sections/animal. (J–U) Section in situ analysis comparing expression of *Col9a1*, *Col2a1*, *Col10a1*, *Ihh*, *Ptc*, and *Pth1r* between wt and *Mia3*-null 14.5-dpc humeri demonstrates an intact Ihh and Pth1r signaling axis despite dysmorphism of the cartilage. (V and W) Comparison of 14.5-dpc wt and *Mia3*$^{-/-}$ forelimb RNA on Mouse Genome 430 v2.0 arrays (Affymetrix) reveals an overall reduction in genes associated with chondrogenic progression (V) and osteoblast expansion (W; $n = 5$ per group, $P < 0.05$). Expression values are represented as colors, in which the range of colors (red, pink, light blue, and dark blue) shows the range of expression values (high, moderate, low, and lowest). Bars, 100 µm.

by all nonhypertrophic chondrocytes, whereas *Col10a1* expression initiates in prehypertrophic cells and remains up-regulated in mature hypertrophic cells. As anticipated, the onset and amplitude of expression of both collagens in *Mia3*$^{-/-}$ cells lagged behind those of controls. We therefore conclude that Mia3 is required specifically within chondrocytes for their timely maturation.

Consistent with the observation that Col7a1 binds MIA3 and accumulates in cells in which *MIA3* transcripts are reduced by RNAi knockdown (Saito et al., 2009b), comparisons of Col7a1 deposition between wt and *Mia3*$^{-/-}$ MEFs with and without membrane permeabilization reveal a slight reduction in the overall amount of extracellular collagen secreted by the null cells and a dramatic intracellular accumulation of Col7a1 adjacent to the nucleus (Fig. 5 A). The profound and cell-autonomous defects in chondrocyte differentiation, however, suggest a broader role for Mia3 than secretion of Col7a1. Indeed, chondrocyte-enriched primary cell cultures derived from 14.5-dpc *Mia3*$^{-/-}$ ribcages show a similar accumulation of Col2a1 and, to a lesser extent, Col3a1 within the cells (Fig. 5, B and C). Although some collagen is deposited outside of the knockout cells, it appears to be abnormally aggregated and unevenly dispersed throughout the extracellular fibrils. Quantitation of total cell-associated collagen using SDS-PAGE and Western blot analysis confirmed these observations, with 2.2–4.7-fold increases in the amount of Col1, Col3a1, and Col9a1 in *Mia3*-null MEFs relative to controls (Fig. S3, G–I) despite normal levels of transcription (Fig. S3 C). To confirm that these changes were driven by increased retention, we compared ECM-resident versus cell-associated levels of Col1 in chondrocytes and MEFs (Fig. 5 D). A 50% reduction is observed in the amount of ECM-deposited Col1 in *Mia3*-null primary chondrocytes (Fig. 5 E, $P = 0.006$, $n = 3$ per genotype). In MEFs, cell-associated Col1

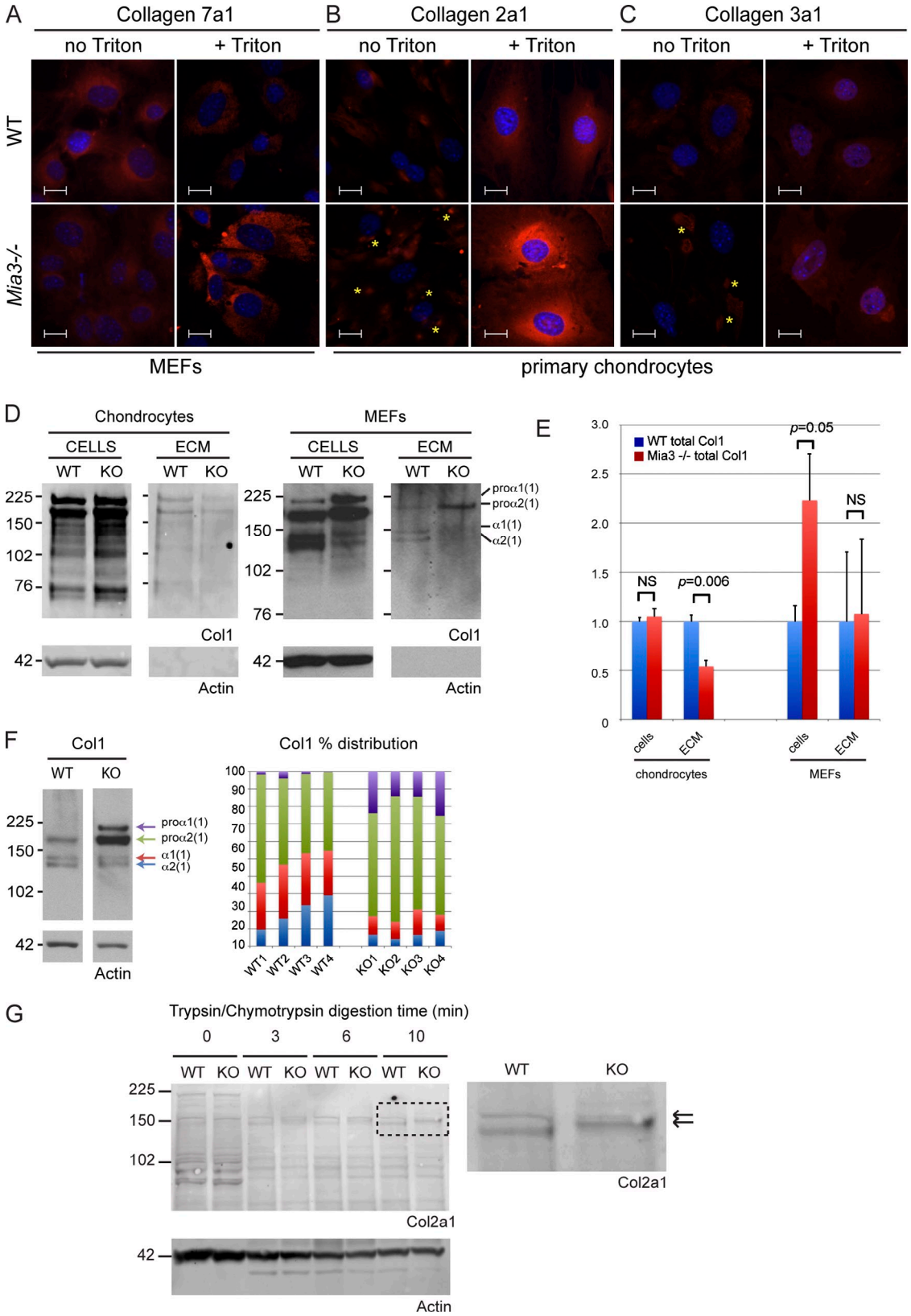

Figure 5. **Abnormal collagen glycosylation, secretion, maturation, and ECM deposition in *Mia3*-null cells.** (A–C) Immunofluorescent staining of wt and *Mia3*$^{-/-}$ primary MEFs (A; Col7a1) and chondrocytes (B and C; Col2a1 and Col3a1) reveals abnormal punctate ECM deposition (asterisks) and an increase in ER-retained collagen upon cell permeabilization. Bars, 10 μm. (D and E) Comparison and quantitation of ECM and cell-associated collagens isolated from wt and *Mia3*-null chondrocytes (left) and MEFs (right). Values are ± SEM. *n* = 3 per genotype. KO, knockout. (F) Western blot analyses of cell-associated collagen 1 (Col1) from wt and *Mia3*$^{-/-}$ MEFs show substantial changes in collagen processing in null cells. Distribution plots summarize data (*n* = 4 per genotype). Arrows indicate processed collagen types. (G) Timed protease digestion of embryonic lysates blotted for Col2a1 further highlights the presence of alternately modified collagen (arrows and boxed region) in *Mia3*-null tissues. Molecular masses are given in kilodaltons.

is increased twofold in Mia3-null cells (P = 0.05), whereas the level of ECM-associated collagen is barely detectable and not significantly different (Fig. 5 E). We conclude that the transit of several collagens is hampered by the loss of Mia3, and reduced levels are deposited within the ECM.

These analyses also reveal a pronounced alteration in the maturation of these collagens in embryo and MEF lysates (Fig. 5 F and Fig. S3, D–I). Newly synthesized molecules of procollagen are co-translationally transferred into the ER and modified, and the N-terminal and C-terminal propeptides (N- and C-propeptides) are processed from the collagen helices during or immediately after secretion by the N-terminal proteinase (N-proteinase) Adamts2 and the C-terminal proteinase (C-proteinase) BMP1, respectively (Dombrowski and Prockop, 1988; Li et al., 1996). In *Mia3*-null MEFs, the procollagen forms of Col1a1 and Col1a2 are readily distinguishable and highly enriched when compared with control lysates (Fig. 5 F). These shifts are also observed in embryonic tissue lysates (Fig. S3 E). Enrichment for alternately migrating species of Col3a1 and Col9a1 is also observed in knockout tissues and MEFs (Fig. S3, F–I), but the exact nature of these forms is unresolved. Deglycosylation with peptide-*N*-glycosidase F (PNGase F) reduces the largest Col1 band (Fig. S3 E), suggesting that this is a modified glycoform, and protease-resistant Col2a1 fragments also display altered migration in mutant embryo lysates (Fig. 5 G). These fragments are not detected when samples are predigested with PNGase F (unpublished data), demonstrating that these indeed represent protease-resistant glycoforms. A similar shift in collagen mobility, driven by altered glycosylation and propeptide cleavage, is also observed in cells and tissues lacking the collagen chaperone Hsp47 (Nagai et al., 2000; Ishida et al., 2006). These biochemical analyses are consistent with a delay in the maturation and secretion of several collagens.

To evaluate collagen secretion defects in vivo, we looked at the distribution of collagen in the developing bone at 14.5 dpc. Col2a1 is highly expressed, but extracellular staining is significantly reduced and accompanied by intracellular accumulation in the knockout animals (Fig. 6, A–D). Expression of Col3a1, a prototypical fibrillar collagen, is significantly up-regulated in the mutant chondrocytes but is only detectable intracellularly rather than in the ECM (Fig. 6, E and F). Col1, another fibrillar collagen, is abundantly expressed in the mutant but mislocalized to an intracellular compartment (Fig. 6, G and H). Costaining of the plasma membrane with WGA further emphasizes the significant reduction of Col1 incorporation into extracellular collagen fibrils (Fig. 6, G′ and H′).

Because Mia3 is broadly expressed in all tissues throughout development, we examined the distribution of collagens and other large ECM molecules in other tissues. Col1 and Col3a1 are expressed outside of the bone in skin and the underlying mesenchymal cells. In contrast to the fibrillar staining in control mesenchyme, numerous *Mia3*$^{-/-}$ cells contained intracellular aggregates of these collagens (Fig. 6, I–L). Intracellular accumulation of Col4a1 is apparent throughout the developing *Mia3*$^{-/-}$ vasculature (Fig. 6, M and N), and colabeling with antibodies against MECA-32 (Fig. 6, O and P) and smooth muscle actin (Fig. 6, Q and R) demonstrates that Col4a1 accumulation occurs in both endothelial cells and mural cells. Col4a1 is a major component of the basement membrane of numerous other tissues, and cells nestled between the muscle fibers in *Mia3* knockouts also contain prominent intracellular aggregates of Col4a1 that are absent in controls (Fig. 6, S and T). In contrast, deposition of fibronectin and aggrecan, 440-kD and 2,500-kD ECM proteins, is unaffected, and intracellular accumulation is not observed in vivo (Fig. S4). Fibronectin fibrils are extracellular in the chondrocytes (not depicted) and limb mesenchyme (Fig. S4, A and B). Colabeling of WGA and aggrecan also shows strong extracellular staining (Fig. S4, C and D). Comp (cartilage oligomeric matrix protein), an extracellular collagen-associated protein that has been shown to facilitate fibrillogenesis (Zaucke and Grässel, 2009), also aggregates within the ER of *Mia3*-null chondrocytes (Fig. 6, U–X). However, it is difficult to ascertain whether this is a direct effect. Accumulation of intracellular COMP can result in the coretention of interacting partners, including Col9a1 (Holden et al., 2001), and the reverse phenomenon may be driven by the collagen accumulation in *Mia3* mutant cells. We conclude that Mia3 does not play a general role in facilitating the export of all ECM proteins but, rather, is required for normal collagen secretion and deposition in numerous tissues, including, but not limited to, the bone, skin, muscles, and developing vasculature.

To further investigate how protein accumulation affected *Mia3* mutant cells, we performed transmission EM (TEM) analysis of developing chondrocytes. TEM revealed marked distension of the ER in *Mia3* mutants (Fig. 7, A–D), which is consistent with ER accumulation of collagens in these highly secretory cells. Furthermore, it is well recognized that abnormal accumulation of misfolded proteins in the ER causes ER stress, which triggers the response of the ER quality control system (Ma and Hendershot, 2004). Given the distended ER revealed by TEM and immunofluorescent detection of increased and apparently aggregated collagens in mutant cells, we hypothesized that the unfolded protein response (UPR) might be induced.

Consistent with these morphological changes, gene expression profiling by the microarray of wt and *Mia3*$^{-/-}$ forelimb RNA collected from 12.5-, 13.5-, and 14.5-dpc embryos ($n = 5$ per genotype) reveals a highly significant increase in genes associated with the UPR (Fig. 8 A). These include primary drivers of the UPR, such as CHOP and ATF4, as well as numerous downstream targets, including Grp78/BiP (binding immunoglobulin protein), Atf5, and Dnajb9. Mediators of ER-associated degradation (ERAD), such as Derl1 and Edem1, are also highly up-regulated. The majority of these genes are expressed at normal (low) levels at 12.5 dpc, but their expression begins to diverge from wt littermates at 13.5 dpc (Fig. 8, B and C). This trend was maintained at 14.5 and 16.5 dpc (Fig. S5).

In situ expression analysis of the primary UPR effectors *Atf4*, *Atf5*, and *CHOP1* as well as two targets of the Atf4–CHOP pathway, *Chac1* and *Trb3* (*tribbles homologue 3*; Ohoka et al., 2005; Mungrue et al., 2009) reveals specific up-regulation of the UPR throughout the chondrocytes of the 14.5-dpc limb (Fig. 8, D–M). Extremely low levels of *Atf4* and *Atf5* near the limit of detection were noted in scattered control prehypertrophic

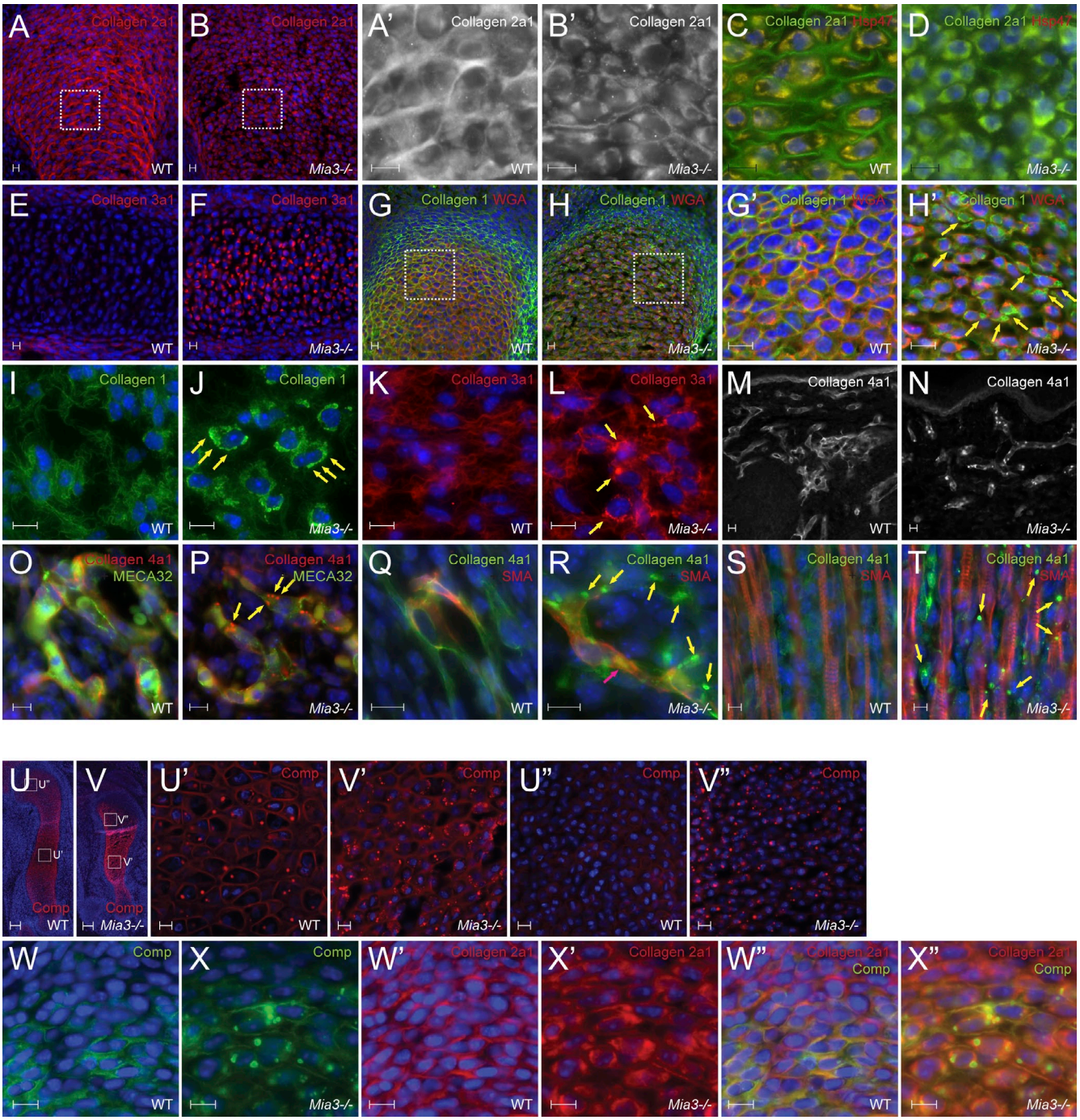

Figure 6. **Collagen and Comp retention and reduced fibril formation in *Mia3*-null embryonic tissues.** (A–H) Matrix deposition of Col2a1 (A–D), Col3a1 (E and F), and Col1 (G and H) is reduced around chondrocytes within 14.5-dpc *Mia3*-null bones. Boxed regions are enlarged in adjacent panels. Col2a1 overlaps exclusively with the ER marker Hsp47 in null chondrocytes (C and D), with similar results seen with Col1 and Col3a1 (not depicted). (G and H) WGA labeling of the plasma membrane reveals intracellular accumulation of Col1 in null cells. Yellow arrows in all panels highlight these collagen aggregates. (I–L) Deposition of Col1 (I and J) and Col3a1 (K and L) within collagen fibrils is reduced in *Mia3*-null subdermal mesenchymal cells with associated intracellular accumulation. (M and N) Vascular Col4a1 is present within intracellular aggregates in the *Mia3* knockouts. (O–R) Colabeling of Col4a1 and MECA-32 (O and P) or smooth muscle actin (Q and R) demonstrates abnormal collagen accumulation within both endothelial (yellow arrows) and mural cells (pink arrow) of the limb vasculature. (S and T) Col4a1 is disrupted in the basement membrane of the *Mia3* mutant muscle. (U–V″) Comp is predominantly ECM associated in wt hypertrophic chondrocytes (enlarged in U′) and resting chondrocytes (U″) of the 14.5-dpc humerus, whereas in *Mia3*$^{-/-}$ cartilage condensates, COMP is found both within and without the hypertrophic chondrocytes (V′) and is predominantly intracellular in the growth plate (V″). (W–X″) Antibody labeling of Comp intracellular aggregates (W and X) and Col2a1 aggregates (W′ and X′) within *Mia3*-null chondrocytes overlaps (W″ and X″) with cell-retained Col2a1, indicating that both factors are trapped within the ER. Bars: (A–T and W–X″) 10 µm; (U–V″) 100 µm.

cells (Fig. 8, D and F; and not depicted) as well as dermal fibroblasts. These general trends in expression also hold true at 16.5 dpc (Fig. S5) with two exceptions: *Atf5* becomes apparent in the knockout epidermis and dermis (Fig. S5 L), and *CHOP1* expression also becomes significantly up-regulated in the *Mia3*-null prehypertrophic chondrocytes (Fig. S5 M). These results were

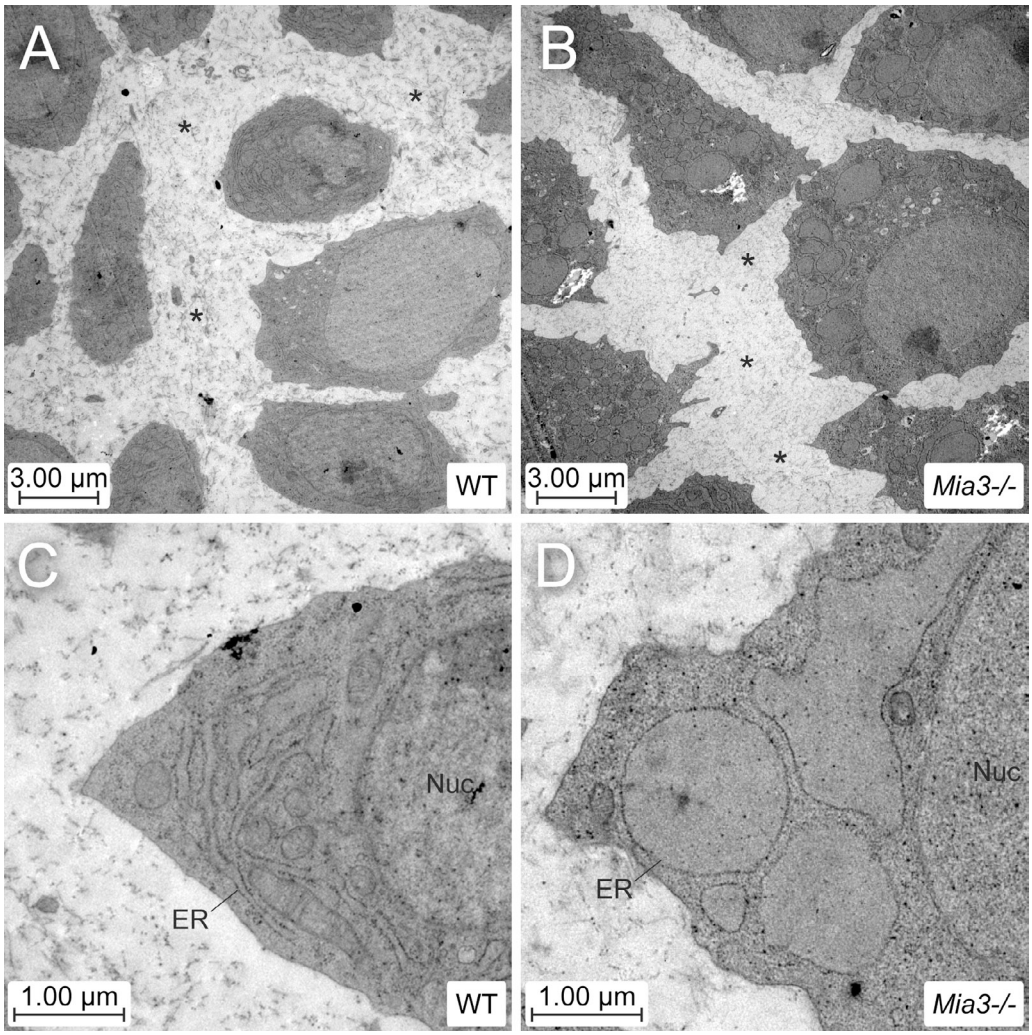

Figure 7. **The endoplasmic reticulum is grossly distended, and collagen fibrils are reduced in knockout chondrocytes.** (A–D) Comparative TEM images of wt (A and C) and *Mia3* mutant (B and D) proliferative zone chondrocytes within the humerus. ER distention is clearly evident in the majority of null cells along with a concomitant reduction in extracellular collagen fibril assembly (asterisks). Nuc, nucleus.

further corroborated at 16.5 dpc using UPR PCR arrays (Fig. S5 O). Thus, we see a relatively uniform up-regulation of UPR genes throughout the *Mia3*-null cartilage template at 14.5 dpc, a pattern that is maintained through 16.5 dpc.

Discussion

We have found that loss of function of the ER-resident protein *Mia3* leads to developmental defects primarily affecting the embryonic skeleton and skin (Fig. 9). We demonstrate that in mutant embryos and primary cell lysates, secretion of numerous collagens, including collagens I, II, III, IV, VII, and IX, is disrupted, most likely because of defective export from the ER. Collagen fibrils, though dispersed and diminished in number, are present in the knockout ECM, and a reduced amount of ECM-associated collagen is discernible by Western blotting and immunofluorescence. This reduction, in turn, leads to a delay in chondrogenesis, and the embryonic null phenotype resembles an amalgam of chondrodysplastic disorders arising from defective collagen folding, deposition, and/or maturation.

The *Mia3* mutant phenotype indicates a high level of specificity in the selection, packaging, and exit of cargo from the ER. Our analysis provides direct evidence that Mia3 is required for proper secretion of all three primary classes of collagens. These include interstitial fibrillar collagens (I, II, and III), a nonfibrillar basement membrane collagen (IV), and a FACIT (fibril-associated collagen with interruptions in triple helix; IX). The fibrillar collagens are major constituents of the ECM that support body structure. Nonfibrillar Col9a1 is exclusively found in basement membranes and provides a scaffold for other ECM components. FACITs associate with the surfaces of fibrillar collagens and mediate their interactions with other ECM proteins. Although distinct in structure, function, and localization, each of these collagen classes contain the characteristic Gly-X-Y triplet repeats that drive the formation of the unique collagen triple helix. Because the N-terminal luminal SH3 domain of Mia3 was shown to bind to Col7a1 (Saito et al., 2009b), we believe this domain, or an associated protein, recognizes the triple helical collagen motif and is responsible for collagen specificity.

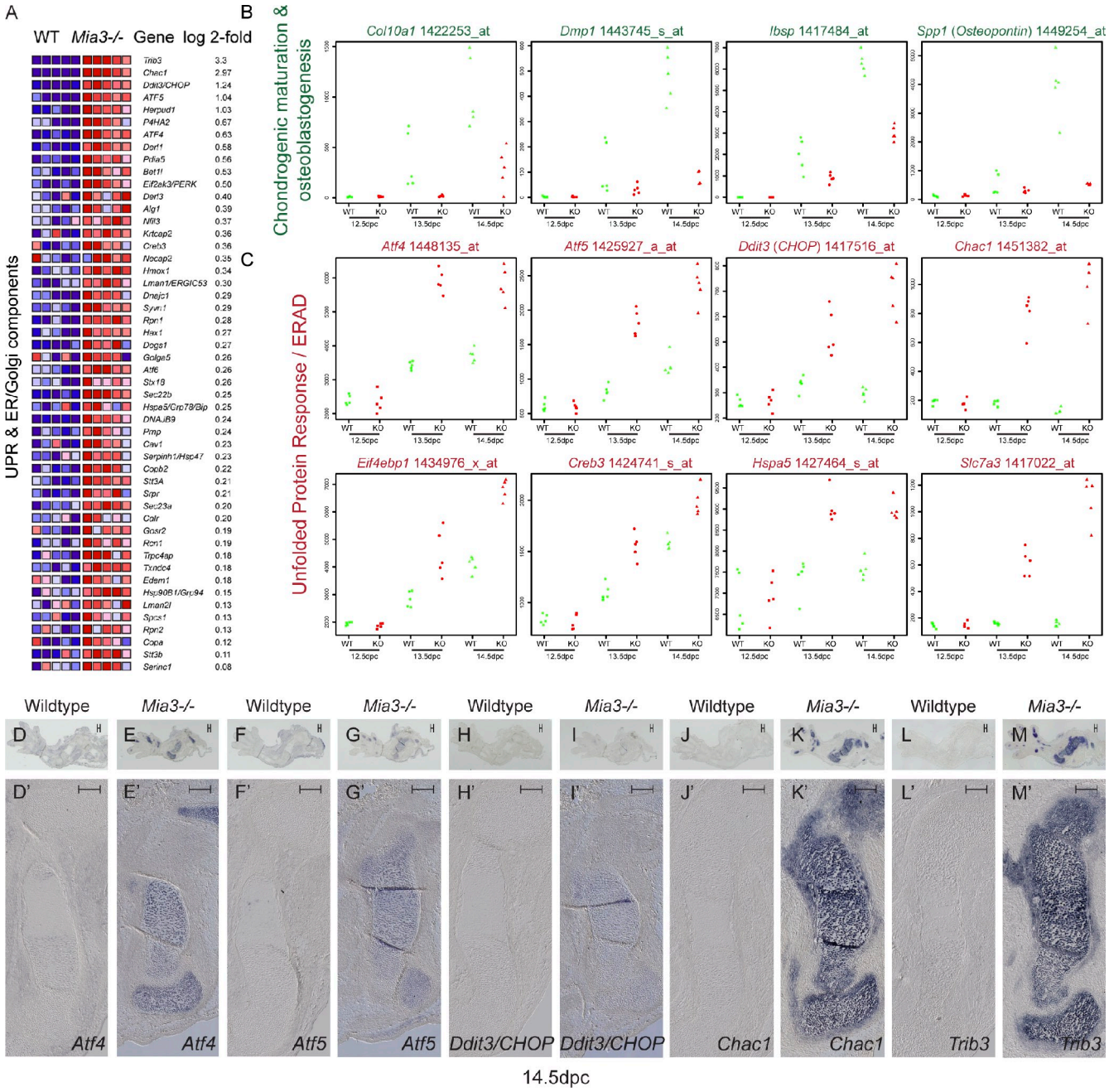

Figure 8. **The UPR is up-regulated in chondrocytes of *Mia3*-null animals coincident with delayed bone maturation.** (A) Gene expression in wt and *Mia3*-null 14.5-dpc limbs ($n = 5$ each) was studied by Mouse Genome v2.0 arrays (Affymetrix) with probes for over 39,000 transcripts. Using unsupervised gene ontology analysis (Broad Institute, Cambridge, MA), over-represented patterns of genes associated with ER and Golgi function/UPR/ERAD were identified. All data presented have a $P < 0.05$. (B and C) Comparison of array data for several probes specific to chondrogenic/osteogenic progression (B; *Col10a1*, *Dmp1*, *Ibsp*, and *Spp1*) and UPR/ER stress (C; *Atf4*, *Atf5*, *Ddit3*, *Chac1*, *Eif4ebp1*, *Creb3*, *Hspa5*, and *Slc7a3*) in 12.5-, 13.5-, and 14.5-dpc whole forelimbs. Misregulation of both gene sets in mutants is concomitant at 13.5 dpc. *Col10a1* and the UPR gene set are significantly misregulated ($P < 0.05$) at 13.5 dpc, whereas the osteogenic markers *Dmp1*, *Ibsp*, and *Spp1* achieve significance at 14.5 dpc. GEO Datasets accession numbers are given at the top. (D–M′) Section in situ hybridization of 14.5-dpc humeri from wt and *Mia3*-null embryos using probes against *Atf4*, *Atf5*, *Ddit3*, *Chac1*, and *Trib3* reveals prominent staining throughout all chondrocytes in comparison to controls. D′–M′ denotes close-ups from the humeri shown in D–M. Bars, 100 µm.

Mia3 is a member of a gene family defined by the unique presence of an extracellular SH3 domain. The other three family members encode small (~100 amino acid) secreted proteins (Mia1, Mia2, and Otor; Lougheed et al., 2001). Work by Saito et al. (2009b) as well as our own experiments indicates that the ER-resident Mia3 represents a divergent, membrane-anchored member of this gene family. Interestingly, despite this structural divergence, other members of the Mia family are also suggested to have roles regulating chondrogenesis. For example, *Otor* expression is restricted to the cartilaginous cells of the developing cochlea (Robertson et al., 2000) and required for their differentiation (Cohen-Salmon et al., 2000). Similarly, *Mia1* is expressed exclusively in the developing skeleton, and *Mia1*-null mice are viable and display subtle ultrastructural defects in collagen fibril

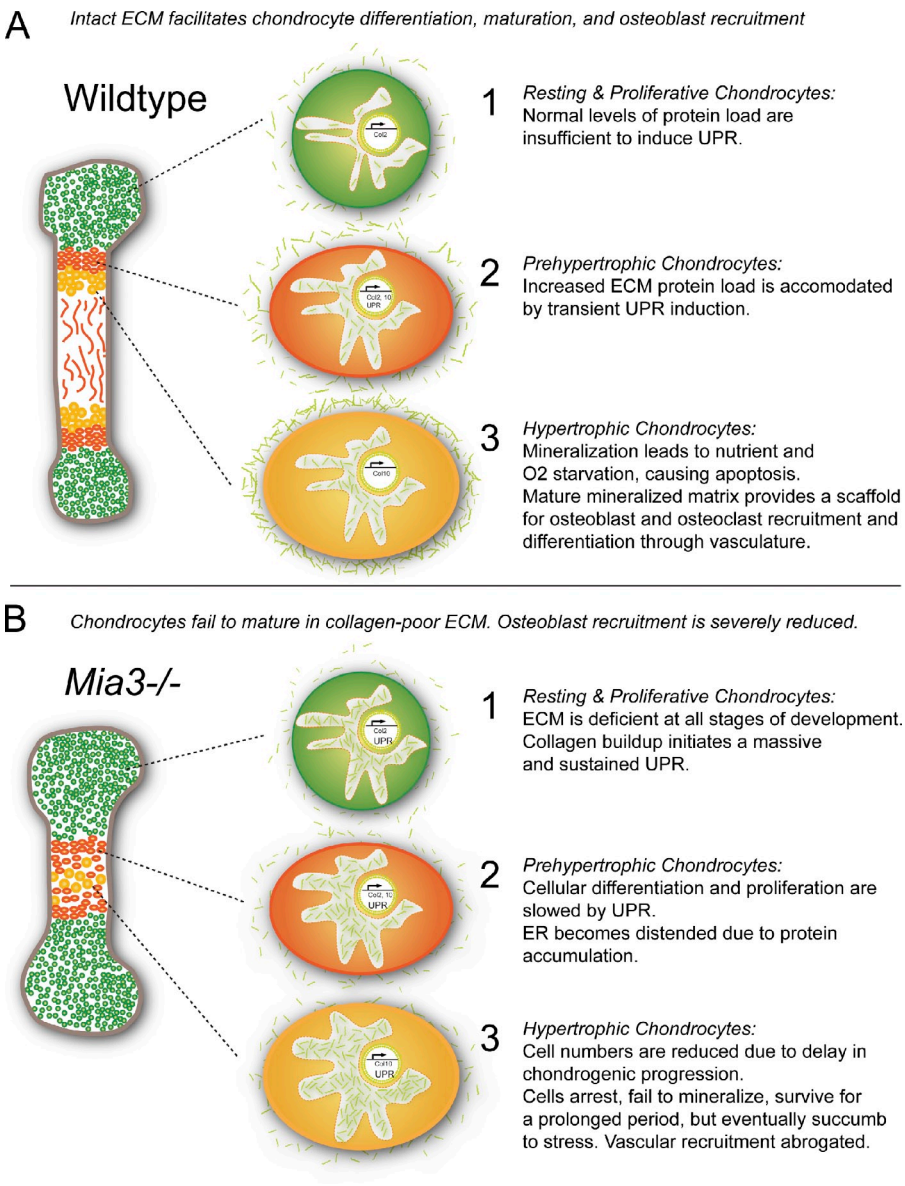

Figure 9. **A schematic for the interaction between Mia3 and the UPR machinery in regulating collagen metabolism as modeled in chondrocytes.** (A) In wt animals, the normally low levels of UPR regulators are sufficient to handle the increase in protein load during chondrocyte maturation. (B) The loss of Mia3 rapidly leads to buildup and retention of collagen within the ER and initiates a strong and sustained UPR that is sufficient to slow cellular differentiation and prevent generalized apoptosis.

assembly (Moser et al., 2002). Recombinant Mia1 binds to the ECM components fibronectin and laminin and shows an affinity for tenascin and Col9a1 (Bosserhoff et al., 2003). Each of these proteins contains a characteristic exposed arginine-glycine-aspartic acid tripeptide-repeating motif (a specific derivative of the Gly-X-Y collagen helical motif), and purified Mia1 can bind this motif in isolation. We suggest that the unique MIA family SH3 fold represents a conserved motif that has evolved to modulate collagen metabolism both within the cell, during packaging and secretion, as well as outside of the cell, during incorporation into the ECM.

Distinct from the other Mia proteins, Mia3 has a hydrophobic transmembrane domain and C-terminal proline-rich region. The C-terminal domain interacts with SEC24C, a core component of the COPII coat protein complex. The COPII complex is responsible for the initiation of vesicle formation, cargo selection, polymerization, and release of loaded carriers from ER membranes (Barlowe et al., 1994). COPII consists of five core proteins (Sar1, Sec13, Sec31, Sec23, and Sec24), and mutations in Sec13, Sec23, and Sec24 cause chondrodysplastic phenotypes (Boyadjiev et al., 2006; Lang et al., 2006; Fromme et al., 2007; Townley et al., 2008; Ohisa et al., 2010; Sarmah et al., 2010). In each of these genetic models, collagen export in mutant cartilage is blocked and the ER becomes engorged, but transport and secretion of smaller proteins remain unchanged. Because the interaction of SEC24C is hypothesized to be critical for MIA3-facilitated loading into ER export vesicles (Saito et al., 2009b), we suggest that the proper coupling of Sec13–Sec31 to Sec23–Sec24 is required for the secretion of large macromolecular cargo from the ER. Chondrocytes, because they secrete substantial amounts of ECM, are especially sensitive to perturbations in protein traffic. Therefore, it is intriguing that we have identified a shorter isoform of Mia3 that consists of only the transmembrane and C-terminal Sec24c-interacting domains. Expression of this isoform is not disrupted in our mutant, and we can only speculate about its function. Because it lacks the collagen-interacting SH3 domain, it may serve to modulate or sequester Sec24c rather than directly regulating collagen export from the ER.

The presence of high molecular mass forms of collagen in *Mia3*-null lysates (Fig. 5 and Fig. S3) supports our hypothesis that processing (cleavage) of collagen propeptides is impaired in *Mia3*-null cells, much as it is in *Hsp47*-null mice (Nagai et al., 2000; Ishida et al., 2006). The clearest example of this phenomenon is seen with Col1 in which there is a pronounced shift in the amount of procollagen observed in knockout cells (Fig. 5, E and N). In some examples of osteogenesis imperfecta, mutations within the triple helical domain of COL1A1 prevent N-propeptide cleavage (Vogel et al., 1987, 1988), leading to similar shifts in migration. Col3a1 and Col9a1 also display these mobility shifts. Higher molecular mass bands are enriched, but their identity remains to be clarified. We believe these differences are significant, especially for Col9a1, because the higher molecular mass form is consistently and dramatically enriched in *Mia3*-null cells (Fig. S3 H). Thus, Mia3 is required for timely collagen maturation and secretion.

Clearly, Mia3 is not absolutely required for collagen secretion, as not all collagens are affected to the same extent in all tissues by the loss of Mia3. For example, extracellular Col2a1 fibrils are almost nonexistent in the null cartilage (Fig. 6, C and D), whereas fibrils containing Col3a1 still surround mesenchymal cells despite ER accumulation (Fig. 6, K and L). Our Western blot analyses also confirm that collagen secretion indeed still occurs in *Mia3*-null cells (Fig. 5 and Fig. S3). Either an alternate independent pathway of egress remains open to large ECM cargoes, or these proteins can still exit via large COPII vesicles.

It is possible that Mia3 may also play a role in the export of other proteins. Recent studies reveal that the Sec24 cargo adapters bind preferentially to different ER export signals (Wendeler et al., 2007; Mancias and Goldberg, 2008), whereas several export signals are recognized redundantly by two or more of the Sec24 isoforms. The only noncollagen protein that we found to accumulate in the ER of *Mia3*-null chondrocytes is COMP (Fig. 7). COMP is a large glycoprotein found predominantly in the ECM of cartilage and interacts with both fibrillar and nonfibrillar collagens with high affinity. COMP knockout mice show normal development, growth, and longevity, so it is clearly not required for collagen secretion (Hecht et al., 1998). Because collagen ER exit is disrupted in *COMP* mutants (Holden et al., 2001) and both aggregate within the *Mia3*-null ER, it is likely that the retention of COMP is secondary to the retention of collagens.

In the absence of Mia3, collagen buildup within the chondrocyte ER initiates the UPR (Fig. 9). The UPR machinery is required not only to police misfolded proteins but also to deal with the episodic changes in protein load occurring during normal developmental processes. The observation that the UPR mediators *Atf4*, *Atf5*, and *Trb3* are present, albeit at low levels, in normal prehypertrophic cells indicates that maturing chondrocytes normally induce their expression, likely because of the increasing demand on the ER/Golgi as chondrocytes create and embed themselves in a collagen-rich ECM (Eyre, 2004). Indeed, loss of function mutations in PERK (eukaryotic initiation factor 2 α kinase) cause defects in highly secretory cells, such as osteoblasts and exocrine cells of the pancreas (Zhang et al., 2002), and Atf4, one of the primary effectors of the UPR cascade below PERK and Eif2α, is also required for osteoblast differentiation and function (Yang et al., 2004). Combined activation of Ire1, PERK, and ATF6 produces cytoprotective outputs, such as reduced translation, enhanced ER protein-folding capacity, and clearance of misfolded ER proteins along with proapoptotic outputs, such as CHOP production. Although CHOP is up-regulated in the prehypertrophic chondrocytes of *Mia3* mutants, we believe that the simultaneous up-regulation of *Ire1* (as indicated by its targets Grp78/BiP and DNAJB9) and *Atf6* (Fig. 9) is cytoprotective, and apoptosis is averted early in the elaboration of the phenotype (Fig. 4, E–H). However, the developmentally arrested chondrocytes begin to succumb and show evidence of apoptosis and necrosis by 18.5 dpc (Fig. 3, N and N′).

BBF2H7 is another ER resident basic helix-loop-helix transcription factor that is highly expressed in chondrocytes, activated by ER stress, and is, itself, an activator of Sec23a expression (Kondo et al., 2007). Thus, acting via Bbf2h7, ER stress can activate ER to Golgi trafficking, specifically in the cartilage, and this induction is required to handle normal ECM protein load in chondrocytes. Intriguingly, *Bbf2h7*$^{-/-}$ mice are phenotypically indistinguishable from *Mia3*$^{-/-}$ mice (Saito et al., 2009a).

Recent association studies have demonstrated a link between polymorphisms at the *MIA3* locus and early onset MI (Samani et al., 2007; Kathiresan et al., 2009). The underlying pathobiology of MI is a buildup of atherosclerotic plaques on the walls of major vessels, with plaque rupture and ensuing thrombosis being responsible for the majority of cases (Schoenhagen et al., 2002). Collagens constitute ∼60% of the protein of an atherosclerotic plaque (Smith, 1965), and the collagen-rich fibrous cap covering the lipid-dense core of the atherosclerotic plaque is the major factor in its stability (Adiguzel et al., 2009). It is exciting then that our experiments provide a plausible biological mechanism and potential model for MIA3's involvement in MI. An imbalance between collagen synthesis and degradation by macrophage- and smooth muscle cell–associated proteinases could lead to cap thinning, degradation of the collagen IV–enriched basement membrane, and plaque instability. A straightforward prediction from our studies is that a reduction in *MIA3* expression would tilt the balance toward a thinner cap and an unstable plaque.

Materials and methods

Animals

Mia3$^{+/-}$ mice were backcrossed and maintained on a C57BL/6 background. Intercrosses between heterozygous offspring were used to obtain *Mia3*$^{-/-}$ embryos. Yolk sac– or embryonic tissue–derived genomic DNA was genotyped by PCR in which primers specific for wt or mutant alleles were combined in the same reaction. Genotyping of *Mia3* knockout mice was performed by PCR using primers directed against neomycin, 5′-GCAGCGCATCGCCTTCTATCG-3′; intron 1, 5′-AAGACCGTGTCTGTGGCTCAG-3′; and intron 2, 5′-GCACCACCACCACCAAGAGTT-3′, which generates a 380-bp product in the wt and a 232-bp product in the knockout allele. The reaction conditions were 94°C for 4 min followed by 30 cycles at 94°C for 30 s (denaturing), 62°C for 1 min (annealing), and 72°C for 1 min (extension). Noon of the day of vaginal plug detection was termed 0.5 dpc. All animals were handled in accordance with protocols approved by the Genentech Institutional Animal Care and Use Committee. Mouse colonies were maintained in a barrier facility at Genentech, conforming to California state legal and ethical standards of animal care.

Cell culture

MEFs were harvested from eviscerated and beheaded 12.5 dpc embryos by digestion with 0.05% trypsin-EDTA in PBS overnight at 4°C, dissociated by triturating, plated (one embryo per T75), and maintained in 10% FBS DME with penicillin/streptomycin for 2 d. MEFs were then passaged for experimentation no more than five times. Primary chondrocytes were harvested from 14.5-dpc embryonic ribcages by digestion with 5× trypsin-EDTA in PBS for 1 h with hard vortexing every 15 min. Subsequently, the solution was changed to 1 mg/ml collagenase and trypsin in 1% FBS DME for 6 h at 37°C. The digestion was vortexed for 30 s, debris settled for 3 min, and supernatant with suspended cells was plated. Media were changed to 5% FBS α-MEM containing 1 mM β-glycerolphosphate and insulin-transferrin-selenium A (Invitrogen) for the duration of the experiment.

ECM harvesting

Primary chondrocytes or MEFs were harvested as described (see the previous paragraph) and grown on 10-cm plates for 10 or 3–4 d, respectively. 50 µg/ml ascorbic acid (Alfa Aesar) was added fresh to the media each day to stimulate collagen transcription. To produce cell lysates, cells were incubated for 15 min at 37°C with 1 ml of either 1-M NaCl or 0.5% deoxycholate in PBS and sonicated. Plates were washed several times with 0.5% deoxycholate at 37°C followed by ice-cold PBS to remove all cells and ECM extraction buffer (5% SDS and 100 mM Tris, pH 6.8) for 15 min. ECM was scraped from the plate and heated at 96°C for 10 min. Protein concentrations of cell lysates were determined using bicinchoninic acid reagent (Thermo Fisher Scientific). For analysis by Western blotting with anticollagen antibodies (Table S1), equal amounts of ECM were calculated based on cell lysate concentrations, and equal quantities of cell lysate samples were loaded.

Histology

For all section in situ and histological/immunohistological analyses, mouse embryos were fixed by immersion in 4% paraformaldehyde in PBS and processed for paraffin sections at 10 µm. Masson's trichrome stain and regressive hematoxylin and eosin stains were run on samples collected in Bouin's fixative as per standard protocols. Alcian blue/Alizarin red skeletal preparations were processed as previously described (Solloway et al., 1998). For immunofluorescent and immunohistochemical staining, the primary antibodies used are outlined in Table S1, fluorescent secondary antibodies were conjugated with Alexa Fluor 488 or 549 (1:500; Invitrogen), and peroxidase staining was visualized using the Vectastain ABC kit (Vector Laboratories), whereas rabbit antibodies were visualized with DAB (Thermo Fisher Scientific) using the EnVision Plus system (Dako). In situ hybridizations were performed essentially according to the textbook method with minor modifications for slides. Preparation of digoxigenin-labeled RNA probes was performed according to the manufacturer's instructions (Roche). Antisense riboprobes were constructed using the following templates: *Col9a1*, *Chac1*, *Pth1r*, *Trb3*, *Ddit3/Chop*, *Atf4*, and *Atf5*. Specific information is outlined in Table S2. The probes for *Ihh* and *Ptc* were gifts from A. McMahon (Harvard University, Cambridge, MA), whereas *Col2a1*, *Col10a1*, and *osteopontin* were gifts from H.M. Kronenberg (Massachusetts General Hospital, Harvard Medical School, Boston, MA).

Section TUNEL was performed using a colorimetric kit (DeadEnd; Promega). BrdU cell proliferation analysis was performed as previously described (Kim et al., 2001). Image capture of section in situ hybridization and immunohistochemistry was performed using differential interference contrast microscopy on a microscope (Axioskop Plus; Carl Zeiss). Bright-field and dark-field image capture of whole-mount embryo and skeletal preparations were accomplished using a stereomicroscope (Discovery. V12; Carl Zeiss) and Axiovision AC software (version 4.4; Carl Zeiss).

Immunofluorescence

Cells at ∼80% confluence were washed in PBS, fixed in ice-cold 4% paraformaldehyde for 10 min, and blocked in 3% donkey serum PBS with or without 0.1% Triton X-100 at 4°C for 1 h. The cells were incubated with primary antibodies in 1 mg/ml BSA in PBS with or without 0.1% Triton X-100 at 4°C overnight followed by washing and detection with Alexa Fluor dye–conjugated secondary antibodies (Invitrogen). Images were captured on an upright wide-field fluorescence microscope (BX-61 [Olympus] or Axioskop Plus) using SlideBook (Intelligent Imaging Innovations, Inc.) or Axiovision version 4.6 software, and acquired data were normalized using standard parameters in Photoshop (CS3; Adobe). Raw tiff data were overlaid into separate color channels, composited, and cropped using Photoshop. Identical settings were used for fluorescence excitation, image capture, and level adjustment for all comparative analyses. Figures were created in Illustrator (CS3; Adobe).

Cellular proliferation

Cellular proliferation was evaluated using the Tissue Studio analysis suite in Definiens Architect v1.3 image analysis software (Definiens AG). Regions of interest, defined as each growth plate of a humerus, were identified and manually circumscribed in digital micrographs acquired on a microscope (Axioskop 2 plus [Carl Zeiss]; 20× magnification and 2.4 pixels/µm) from 10-µm paraffin sections. Two wt and three knockout animals were examined (n = between 4 and 10 growth plates per animal). Hematoxylin-positive nuclei were segmented and quantified, with a subset of proliferating nuclei identified using an empirically determined fixed threshold for DAB/Ki67 (Thermo Fisher Scientific) positivity. A proliferation index was then calculated as the ratio of proliferating to total nuclei in each defined region of interest.

TEM

The tissues were fixed in 1/2-strength Karnovsky's fixative (2% paraformaldehyde and 2.5% glutaraldehyde in 0.1 M sodium cacodylate buffer, pH 7.2), washed in the same buffer, and postfixed in 1% aqueous osmium textroxide for 1 h. The samples were then dehydrated through a series of ethanol followed by propylene oxide and embedded in Eponate 12 (Ted Pella). Thin sections were cut on a microtome (Ultracut E; Reichert), stained with uranyl acetate and lead citrate, and examined in a microscope (CM12; Philips). Images were captured with a retractable digital camera (MultiScan; Gatan).

Micro-CT acquisition and image analysis

Mouse fetuses were imaged ex vivo in a hydrated scanning tube with an x-ray micro-CT system (µCT 40; SCANCO Medical). The micro-CT images were generated by operating the x-ray tube at an energy level of 45 kV, a current of 177 µA, and an integration time of 450 ms. Axial images were obtained at an isotropic resolution of 15 µm. The micro-CT scans were analyzed with Analyze software (AnalyzeDirect, Inc.). Maximum-intensity projections and 3D surface renderings in the sagittal plane were created. The mouse tissue was segmented from the scanning tube and noise with a low threshold, whereas the mineralized skeleton was segmented from the rest of the fetus with a higher threshold plus an erosion–dilation.

RT-PCR and TaqMan

For RT-PCR, total RNA was isolated from embryonic day 14.5 mice using TRIZOL reagent (Invitrogen) and subsequent DNase treatment. RT-PCR was performed using an RT-PCR kit (Superscript III; Invitrogen) and using the following primers to demonstrate the presence of exon4 in *Mia3*-null embryos: *exon1–4* forward, 5′-AAAGTGGCGGGGACGAAGAG-3′, and reverse, 5′-AAAGCACCTTCTCCATCCTCTG-3′, and *exon1B* forward, 5′-ATGGAAGGTGGTCCTGTTGGG-3′, and reverse, 5′-CCAGGGCAGTCCGTAAAAGTC-3′, at 55°C for 30 min (cDNA synthesis) and 95°C for 2 min followed by 25 cycles of 95°C for 15 s (denaturation), 60°C for 30 s (annealing), and 68°C for 30 s (elongation). To determine whether *Mia3* is up-regulated in response to stress, the following primers were used: *Mia3 5′* forward, 5′-AGCCACGGACGGCGTTTCTC-3′, and reverse, 5′-ATCCCCCTGCCAGTTTGTAGTA-3′; *Hspa5* forward, 5′-ACCTGGGTGGGGAAGACTTTG-3′, and reverse, 5′-GCTCTTCAAATTTGGCCCGAGT-3′; and *Gapdh* forward, 5′-ATGGTGAAGGTCGGTGTGAACG-3′, and reverse, 5′-TCACCCCATTTGATGTTAGTGGG-3′. Cycling conditions were as follows: 55°C for 30 min (cDNA synthesis) and 95°C for 2 min followed by 25 cycles of 95°C for 15 s (denaturation), 60°C for 30 s (annealing), and 68°C for 30 s (elongation). For TaqMan, MEFs were resuspended in growth media at 100,000 cells per 20 µl. 20 µl of dots was plated, allowed to dry for 15 min, and then flooded with 1 ml growth media. 50 ng/ml BMP2 (R&D Systems) treatment was performed on the following day. Cells were frozen at day 0 (no bone morphogenic protein), 1, 4, 9, and 12. RNA was then extracted using the RNeasy kit (QIAGEN) according to the manufacturer's instructions. cDNAs were generated using the Cells-to-Ct kit (Applied Biosystems). 1 µg of each RNA was used per 100-µl reaction, and 10 µl of each cDNA was used for each TaqMan reaction. Specific TaqMan primer/probe sets are outlined in Table S3.

Gene expression microarray studies, analysis, and quantitative PCR

Total RNA was obtained from the forelimbs of 12.5-, 13.5-, 14.5-, and 16.5-dpc embryos using the RNeasy Mini kit (QIAGEN). The manufacturer's protocol was followed for all steps, and the optional on-column DNase treatment was performed. For microarray analyses, RNA was quantified using ultraviolet spectrophotometry. RNA was labeled for and hybridized to expression microarray assay (HGU133; Affymetrix) using standard GeneChip protocols (Affymetrix). At each time point, genes

differentially expressed between mutant and wt were identified using a modified *t* test with Bayesian variance estimate (Baldi and Long, 2001). False discovery rates were estimated by the q-value method of Storey and Tibshirani (2003). Gene set enrichment analysis was performed using Gene Ontology gene sets and "curated" gene sets from the Molecular Signature Database (Subramanian et al. 2005). Statistical significance of the enrichment score was calculated by permuting the gene sets. Quantitative PCR using 16.5-dpc forelimb RNA was performed for an array of osteogenesis and UPR markers according to the manufacturer's recommendations (SA Biosciences). All data presented have a $P < 0.05$ with $n = 3$ samples per genotype.

Mia3 (SH3) protein production and antibody generation

C-terminal FLAG-tagged expression vectors for several different length N-terminal Mia3 fragments were expressed in CHO cells and purified over anti-FLAG beads, but appreciable protein expression was only found for the SH3 domain. This protein as well as a C-terminal peptide (CEMALQKKLSQEEYERQD) was conjugated to keyhole limpet hemocyanin and used to generate affinity-purified rabbit polyclonal antibodies according to standard protocols (Antibody Solutions). Sera were confirmed to be immunopositive by ELISA. The anti-SH3–purified polyclonal antibody was further purified over embryo powder from *Mia3*-null embryos to remove nonspecific cross-reactivity.

Biochemical analyses

Cells were quickly rinsed with PBS and immediately lysed in radioimmunoprecipitation assay buffer plus protease inhibitor cocktail, or embryos were dounce homogenized in radioimmunoprecipitation assay. Protein concentrations were determined using bicinchoninic acid reagent (Thermo Fisher Scientific). Whole lysates were separated by 3–8 or 4–12% SDS-PAGE (Bis-Acetate Gel system; Invitrogen) and transferred onto a nitrocellulose membrane (Millipore) followed by either (a) fluorescence-conjugated secondary antibodies (Invitrogen) for direct scanning using the a phosphoimager (Typhoon; GE Healthcare) and quantification with ImageQuant TL software (GE Healthcare) or (b) HRP-conjugated secondary antibodies (GE Healthcare) for standard enhanced chemiluminescence detection. After the development of exposed films (Kodak), high resolution grayscale scans were collected using a scanner (Scanjet 8200; Hewlett-Packard) and imported into ImageJ (National Institutes of Health) for quantitation using the gel analysis method outlined in the ImageJ documentation. In summary, gel lanes were defined and profiled, and the area corresponding to each band was calculated after the background correction in ImageJ. Results were imported into Excel 2008 (Microsoft) for normalization and subsequent statistical analysis. $n = 3$–4 per genotype, and means are ± SEM. P-values refer to a two-tailed *t* test with equal variance. Collagen isoform distribution plots were normalized for each sample and plotted as percentages in Excel 2008 (Fig. 5). Collagen digestion and deglycosidation was achieved using PNGase F (New England Biolabs, Inc.) as suggested by the manufacturer. In short, 100 µg embryo lysate was incubated with 10,000 U PNGase F for 30 min at 37°C. For protease digestion, 100 µg embryo lysate was incubated with 0.5 µg each of trypsin and chymotrypsin for 3, 6, or 10 min. 20 µg of digested material was mixed with 4× sample loading buffer, boiled, resolved by SDS-PAGE, and blotted. For mass spectroscopy, immunoprecipitates isolated from wt and *Mia3*$^{-/-}$ 14.5-dpc embryo lysates using the C-terminal polyclonal antibody were subjected to SDS-PAGE, purification, digestion, and mass spectrometry. Scaffold software (Proteome Software, Inc.) was used to display all unique peptides with a 95% confidence level in identification.

Image acquisition and processing

All immunofluorescence data except those in Fig. 6 and Fig. S4 were captured on a microscope (BX61; Olympus). Objectives used in the study were the 20×, 0.75 NA and 40×, 0.90 NA UPlanSApo lenses (Olympus). Data were collected at an ambient temperature. The mountant used for immunofluorescence was ProLong gold antifade reagent (Invitrogen), and the fluorochromes were Alexa Fluor 488, Alexa Fluor 594, and Hoechst 33342 plus DAPI (Invitrogen). Images were acquired using a monocamera (Retiga SRV; QImaging) controlled via SlideBook software v4.2. γ adjustments and overlays of grayscale tiffs were accomplished in SlideBook and Photoshop using standard techniques. All comparative photos throughout this analysis were modified using identical parameters.

Fluorescent images in Fig. 6 and Fig. S4 were captured using a microscope (Axioskop2 Plus). Objectives used in the study were 20×, 0.5 NA and 40×, 0.75 NA Plan Neofluar lenses (Carl Zeiss). Staining, mounting, and capture conditions were identical to those described in the preceding paragraph. Images were acquired using a color camera (AxioCam HRc; Carl Zeiss) controlled via AxioVision v4.8.1 software. γ adjustments and overlays were performed in Photoshop using standard techniques.

All nonfluorescent images were collected on a microscope (SteREO Discovery.V12; Carl Zeiss) with M^2 Bio attachment equipped with an Achromat S FWD 69-mm lens (Carl Zeiss) at an ambient temperature. Skeletons were cleared and mounted in 80% glycerol, whereas in situ hybridizations were permanently mounted using Poly-Mount (Polysciences, Inc.). Images were acquired on an color camera (AxioCam HRc) controlled with AxioVision AC software v4.4.0.0. γ adjustments and composites were performed in Photoshop using standard techniques. Low resolution bone in situ hybridization images were composited from multiple tiff files with a maximal 5–10-cell diameter overlap using Interactive Photomerge.

Online supplemental material

Fig. S1 shows characterization of the Mia3 locus, transcripts, and targeting design. Fig. S2 shows validation of anti-Mia3 polyclonal antibodies. Fig. S3 demonstrates additional expression and metabolism analyses in *Mia3*-null primary cell cultures. Fig. S4 provides a description of normal deposition of fibronectin and aggrecan in *Mia3* knockout tissues. Fig. S5 shows a description of significant UPR/ER stress gene up-regulation in *Mia3*$^{-/-}$ chondrocytes and fibroblasts at 16.5 dpc. Table S1 summarizes antibody reagent data. Table S2 shows in situ probe information. Table S3 shows TaqMan quantitative PCR primer/probes used in this study. Online supplemental material is available at http://www.jcb.org/cgi/content/full/jcb.201007162/DC1.

We gratefully acknowledge the following contributors: Clifford Quan, Phil Haas, and Yvonne Chin for protein production and purification; Jane Winer and Jerry Tang for help with microarray analysis; Laszlo Komuzes for confocal microscopy; and Veronica York for animal care. We would also like to thank Fernando Bazan and Sachdev Sidhu for productive discussions regarding the structure and function of Mia3. We thank Drs. Hank Kronenberg and Andy McMahon for providing several in situ probes used in this analysis.

All authors are employees of Genentech, a member of the Roche group.

Submitted: 28 July 2010
Accepted: 25 April 2011

References

Adiguzel, E., P.J. Ahmad, C. Franco, and M.P. Bendeck. 2009. Collagens in the progression and complications of atherosclerosis. *Vasc. Med.* 14:73–89. doi:10.1177/1358863X08094801

Arndt, S., and A.K. Bosserhoff. 2006. TANGO is a tumor suppressor of malignant melanoma. *Int. J. Cancer*. 119:2812–2820. doi:10.1002/ijc.22242

Arndt, S., and A.K. Bosserhoff. 2007. Reduced expression of TANGO in colon and hepatocellular carcinomas. *Oncol. Rep.* 18:885–891.

Baldi, P., and A.D. Long. 2001. A Bayesian framework for the analysis of microarray expression data: regularized t -test and statistical inferences of gene changes. *Bioinformatics*. 17:509–519. doi:10.1093/bioinformatics/17.6.509

Bard, F., L. Casano, A. Mallabiabarrena, E. Wallace, K. Saito, H. Kitayama, G. Guizzunti, Y. Hu, F. Wendler, R. Dasgupta, et al. 2006. Functional genomics reveals genes involved in protein secretion and Golgi organization. *Nature*. 439:604–607. doi:10.1038/nature04377

Barlowe, C., L. Orci, T. Yeung, M. Hosobuchi, S. Hamamoto, N. Salama, M.F. Rexach, M. Ravazzola, M. Amherdt, and R. Schekman. 1994. COPII: a membrane coat formed by Sec proteins that drive vesicle budding from the endoplasmic reticulum. *Cell*. 77:895–907. doi:10.1016/0092-8674(94)90138-4

Bosserhoff, A.K., R. Stoll, J.P. Sleeman, F. Bataille, R. Buettner, and T.A. Holak. 2003. Active detachment involves inhibition of cell-matrix contacts of malignant melanoma cells by secretion of melanoma inhibitory activity. *Lab. Invest.* 83:1583–1594. doi:10.1097/01.LAB.0000097191.12477.5D

Boyadjiev, S.A., J.C. Fromme, J. Ben, S.S. Chong, C. Nauta, D.J. Hur, G. Zhang, S. Hamamoto, R. Schekman, M. Ravazzola, et al. 2006. Craniolenticulo-sutural dysplasia is caused by a SEC23A mutation leading to abnormal endoplasmic-reticulum-to-Golgi trafficking. *Nat. Genet.* 38:1192–1197. doi:10.1038/ng1876

Cohen-Salmon, M., D. Frenz, W. Liu, E. Verpy, S. Voegeling, and C. Petit. 2000. Fdp, a new fibrocyte-derived protein related to MIA/CD-RAP, has an in vitro effect on the early differentiation of the inner ear mesenchyme. *J. Biol. Chem.* 275:40036–40041. doi:10.1074/jbc.M002876200

Dombrowski, K.E., and D.J. Prockop. 1988. Cleavage of type I and type II procollagens by type I/II procollagen N-proteinase. Correlation of kinetic constants with the predicted conformations of procollagen substrates. *J. Biol. Chem.* 263:16545–16552.

Eyre, D.R. 2004. Collagens and cartilage matrix homeostasis. *Clin. Orthop. Relat. Res.* 427(Suppl.):S118–S122. doi:10.1097/01.blo.0000144855.48640.b9

Fromme, J.C., and R. Schekman. 2005. COPII-coated vesicles: flexible enough for large cargo? *Curr. Opin. Cell Biol.* 17:345–352. doi:10.1016/j.ceb.2005.06.004

Fromme, J.C., M. Ravazzola, S. Hamamoto, M. Al-Balwi, W. Eyaid, S.A. Boyadjiev, P. Cosson, R. Schekman, and L. Orci. 2007. The genetic basis of a craniofacial disease provides insight into COPII coat assembly. *Dev. Cell*. 13:623–634. doi:10.1016/j.devcel.2007.10.005

Hecht, J.T., D. Montufar-Solis, G. Decker, J. Lawler, K. Daniels, and P.J. Duke. 1998. Retention of cartilage oligomeric matrix protein (COMP) and cell death in redifferentiated pseudoachondroplasia chondrocytes. *Matrix Biol.* 17:625–633. doi:10.1016/S0945-053X(98)90113-5

Holden, P., R.S. Meadows, K.L. Chapman, M.E. Grant, K.E. Kadler, and M.D. Briggs. 2001. Cartilage oligomeric matrix protein interacts with type IX collagen, and disruptions to these interactions identify a pathogenetic mechanism in a bone dysplasia family. *J. Biol. Chem.* 276:6046–6055. doi:10.1074/jbc.M009507200

Ishida, Y., H. Kubota, A. Yamamoto, A. Kitamura, H.P. Bächinger, and K. Nagata. 2006. Type I collagen in Hsp47-null cells is aggregated in endoplasmic reticulum and deficient in N-propeptide processing and fibrillogenesis. *Mol. Biol. Cell*. 17:2346–2355. doi:10.1091/mbc.E05-11-1065

Kathiresan, S., B.F. Voight, S. Purcell, K. Musunuru, D. Ardissino, P.M. Mannucci, S. Anand, J.C. Engert, N.J. Samani, H. Schunkert, et al; Myocardial Infarction Genetics Consortium; Wellcome Trust Case Control Consortium. 2009. Genome-wide association of early-onset myocardial infarction with single nucleotide polymorphisms and copy number variants. *Nat. Genet.* 41:334–341. (published erratum appears in *Nat. Genet*. 2009. 41:762) doi:10.1038/ng.327

Kim, R.Y., E.J. Robertson, and M.J. Solloway. 2001. Bmp6 and Bmp7 are required for cushion formation and septation in the developing mouse heart. *Dev. Biol.* 235:449–466. doi:10.1006/dbio.2001.0284

Kondo, S., A. Saito, S. Hino, T. Murakami, M. Ogata, S. Kanemoto, S. Nara, A. Yamashita, K. Yoshinaga, H. Hara, and K. Imaizumi. 2007. BBF2H7, a novel transmembrane bZIP transcription factor, is a new type of endoplasmic reticulum stress transducer. *Mol. Cell. Biol.* 27:1716–1729. doi:10.1128/MCB.01552-06

Kronenberg, H.M. 2003. Developmental regulation of the growth plate. *Nature*. 423:332–336. doi:10.1038/nature01657

Lamandé, S.R., and J.F. Bateman. 1999. Procollagen folding and assembly: the role of endoplasmic reticulum enzymes and molecular chaperones. *Semin. Cell Dev. Biol.* 10:455–464. doi:10.1006/scdb.1999.0317

Lang, M.R., L.A. Lapierre, M. Frotscher, J.R. Goldenring, and E.W. Knapik. 2006. Secretory COPII coat component Sec23a is essential for craniofacial chondrocyte maturation. *Nat. Genet.* 38:1198–1203. doi:10.1038/ng1880

Li, S.W., A.L. Sieron, A. Fertala, Y. Hojima, W.V. Arnold, and D.J. Prockop. 1996. The C-proteinase that processes procollagens to fibrillar collagens is identical to the protein previously identified as bone morphogenic protein-1. *Proc. Natl. Acad. Sci. USA*. 93:5127–5130. doi:10.1073/pnas.93.10.5127

Long, F., X.M. Zhang, S. Karp, Y. Yang, and A.P. McMahon. 2001. Genetic manipulation of hedgehog signaling in the endochondral skeleton reveals a direct role in the regulation of chondrocyte proliferation. *Development*. 128:5099–5108.

Lougheed, J.C., J.M. Holton, T. Alber, J.F. Bazan, and T.M. Handel. 2001. Structure of melanoma inhibitory activity protein, a member of a recently identified family of secreted proteins. *Proc. Natl. Acad. Sci. USA*. 98:5515–5520. doi:10.1073/pnas.091601698

Ma, Y., and L.M. Hendershot. 2004. ER chaperone functions during normal and stress conditions. *J. Chem. Neuroanat.* 28:51–65. doi:10.1016/j.jchemneu.2003.08.007

Mancias, J.D., and J. Goldberg. 2008. Structural basis of cargo membrane protein discrimination by the human COPII coat machinery. *EMBO J.* 27:2918–2928. doi:10.1038/emboj.2008.208

Moser, M., A.K. Bosserhoff, E.B. Hunziker, L. Sandell, R. Fässler, and R. Buettner. 2002. Ultrastructural cartilage abnormalities in MIA/CD-RAP-deficient mice. *Mol. Cell. Biol.* 22:1438–1445. doi:10.1128/MCB.22.5.1438-1445.2002

Mungrue, I.N., J. Pagnon, O. Kohannim, P.S. Gargalovic, and A.J. Lusis. 2009. CHAC1/MGC4504 is a novel proapoptotic component of the unfolded protein response, downstream of the ATF4-ATF3-CHOP cascade. *J. Immunol.* 182:466–476.

Nagai, N., M. Hosokawa, S. Itohara, E. Adachi, T. Matsushita, N. Hosokawa, and K. Nagata. 2000. Embryonic lethality of molecular chaperone hsp47 knockout mice is associated with defects in collagen biosynthesis. *J. Cell Biol.* 150:1499–1506. doi:10.1083/jcb.150.6.1499

Ohisa, S., K. Inohaya, Y. Takano, and A. Kudo. 2010. sec24d encoding a component of COPII is essential for vertebra formation, revealed by the analysis of the medaka mutant, vbi. *Dev. Biol.* 342:85–95. doi:10.1016/j.ydbio.2010.03.016

Ohoka, N., S. Yoshii, T. Hattori, K. Onozaki, and H. Hayashi. 2005. TRB3, a novel ER stress-inducible gene, is induced via ATF4-CHOP pathway and is involved in cell death. *EMBO J.* 24:1243–1255. doi:10.1038/sj.emboj.7600596

Robertson, N.G., S. Heller, J.S. Lin, B.L. Resendes, S. Weremowicz, C.S. Denis, A.M. Bell, A.J. Hudspeth, and C.C. Morton. 2000. A novel conserved cochlear gene, OTOR: identification, expression analysis, and chromosomal mapping. *Genomics*. 66:242–248. doi:10.1006/geno.2000.6224

Saito, A., S. Hino, T. Murakami, S. Kanemoto, S. Kondo, M. Saitoh, R. Nishimura, T. Yoneda, T. Furuichi, S. Ikegawa, et al. 2009a. Regulation of endoplasmic reticulum stress response by a BBF2H7-mediated Sec23a pathway is essential for chondrogenesis. *Nat. Cell Biol.* 11:1197–1204. doi:10.1038/ncb1962

Saito, K., M. Chen, F. Bard, S. Chen, H. Zhou, D. Woodley, R. Polischuk, R. Schekman, and V. Malhotra. 2009b. TANGO1 facilitates cargo loading at endoplasmic reticulum exit sites. *Cell*. 136:891–902. doi:10.1016/j.cell.2008.12.025

Samani, N.J., J. Erdmann, A.S. Hall, C. Hengstenberg, M. Mangino, B. Mayer, R.J. Dixon, T. Meitinger, P. Braund, H.E. Wichmann, et al; WTCCC and the Cardiogenics Consortium. 2007. Genomewide association analysis of coronary artery disease. *N. Engl. J. Med.* 357:443–453. doi:10.1056/NEJMoa072366

Sarmah, S., A. Barrallo-Gimeno, D.B. Melville, J. Topczewski, L. Solnica-Krezel, and E.W. Knapik. 2010. Sec24D-dependent transport of extracellular matrix proteins is required for zebrafish skeletal morphogenesis. *PLoS ONE*. 5:e10367. doi:10.1371/journal.pone.0010367

Schoenhagen, P., E.M. Tuzcu, and S.G. Ellis. 2002. Plaque vulnerability, plaque rupture, and acute coronary syndromes: (multi)-focal manifestation of a systemic disease process. *Circulation*. 106:760–762. doi:10.1161/01.CIR.0000025708.36290.05

Smith, E.B. 1965. The influence of age and atherosclerosis on the chemistry of aortic intima.2. Collagen and mucopolysaccharides. *J. Atheroscler. Res.* 5:241–248. doi:10.1016/S0368-1319(65)80065-5

Solloway, M.J., A.T. Dudley, E.K. Bikoff, K.M. Lyons, B.L. Hogan, and E.J. Robertson. 1998. Mice lacking Bmp6 function. *Dev. Genet.* 22:321–339. doi:10.1002/(SICI)1520-6408(1998)22:4<321::AID-DVG3>3.0.CO;2-8

Stephens, D.J., and R. Pepperkok. 2002. Imaging of procollagen transport reveals COPI-dependent cargo sorting during ER-to-Golgi transport in mammalian cells. *J. Cell Sci.* 115:1149–1160.

St-Jacques, B., M. Hammerschmidt, and A.P. McMahon. 1999. Indian hedgehog signaling regulates proliferation and differentiation of chondrocytes and is essential for bone formation. *Genes Dev.* 13:2072–2086. doi:10.1101/gad.13.16.2072

Storey, J.D., and R. Tibshirani. 2003. Statistical methods for identifying differentially expressed genes in DNA microarrays. *Methods Mol. Biol.* 224:149–157.

Subramanian, A., P. Tamayo, V.K. Mootha, S. Mukherjee, B.L. Ebert, M.A. Gillette, A. Paulovich, S.L. Pomeroy, T.R. Golub, E.S. Lander, and J.P. Mesirov. 2005. Gene set enrichment analysis: a knowledge-based approach for interpreting genome-wide expression profiles. *Proc. Natl. Acad. Sci. USA*. 102:15545–15550. doi:10.1073/pnas.0506580102

Townley, A.K., Y. Feng, K. Schmidt, D.A. Carter, R. Porter, P. Verkade, and D.J. Stephens. 2008. Efficient coupling of Sec23-Sec24 to Sec13-Sec31 drives COPII-dependent collagen secretion and is essential for normal craniofacial development. *J. Cell Sci.* 121:3025–3034. doi:10.1242/jcs.031070

Vertel, B.M., A. Velasco, S. LaFrance, L. Walters, and K. Kaczman-Daniel. 1989. Precursors of chondroitin sulfate proteoglycan are segregated within a subcompartment of the chondrocyte endoplasmic reticulum. *J. Cell Biol.* 109:1827–1836. doi:10.1083/jcb.109.4.1827

Vogel, B.E., R.R. Minor, M. Freund, and D.J. Prockop. 1987. A point mutation in a type I procollagen gene converts glycine 748 of the alpha 1 chain to cysteine and destabilizes the triple helix in a lethal variant of osteogenesis imperfecta. *J. Biol. Chem.* 262:14737–14744.

Vogel, B.E., R. Doelz, K.E. Kadler, Y. Hojima, J. Engel, and D.J. Prockop. 1988. A substitution of cysteine for glycine 748 of the alpha 1 chain produces a kink at this site in the procollagen I molecule and an altered N-proteinase cleavage site over 225 nm away. *J. Biol. Chem.* 263:19249–19255.

Vu, T.H., J.M. Shipley, G. Bergers, J.E. Berger, J.A. Helms, D. Hanahan, S.D. Shapiro, R.M. Senior, and Z. Werb. 1998. MMP-9/gelatinase B is a key regulator of growth plate angiogenesis and apoptosis of hypertrophic chondrocytes. *Cell*. 93:411–422. doi:10.1016/S0092-8674(00)81169-1

Wendeler, M.W., J.P. Paccaud, and H.P. Hauri. 2007. Role of Sec24 isoforms in selective export of membrane proteins from the endoplasmic reticulum. *EMBO Rep.* 8:258–264. doi:10.1038/sj.embor.7400893

Yang, X., K. Matsuda, P. Bialek, S. Jacquot, H.C. Masuoka, T. Schinke, L. Li, S. Brancorsini, P. Sassone-Corsi, T.M. Townes, et al. 2004. ATF4 is a substrate of RSK2 and an essential regulator of osteoblast biology; implication for Coffin-Lowry Syndrome. *Cell*. 117:387–398. doi:10.1016/S0092-8674(04)00344-7

Zaucke, F., and S. Grässel. 2009. Genetic mouse models for the functional analysis of the perifibrillar components collagen IX, COMP and matrilin-3: Implications for growth cartilage differentiation and endochondral ossification. *Histol. Histopathol.* 24:1067–1079.

Zhang, P., B. McGrath, S. Li, A. Frank, F. Zambito, J. Reinert, M. Gannon, K. Ma, K. McNaughton, and D.R. Cavener. 2002. The PERK eukaryotic initiation factor 2 alpha kinase is required for the development of the skeletal system, postnatal growth, and the function and viability of the pancreas. *Mol. Cell. Biol.* 22:3864–3874. doi:10.1128/MCB.22.11.3864-3874.2002